Please use this PDF proof to check the layout of your article. If you would like any changes to be made to the layout, you can leave instructions in the online proofing interface. Making your changes directly in the online proofing interface is the quickest, easiest way to correct and submit your proof. Please note that changes made to the article in the online proofing interface will be added to the article before publication, but are not reflected in this PDF proof.

Mechanical Systems and Signal Processing xxx (xxxx) xxx

Contents lists available at ScienceDirect

Mechanical Systems and Signal Processing

journal homepage: www.elsevier.com/locate/ymssp

A generalized class of uniaxial rate-independent models for simulating asymmetric mechanical hysteresis phenomena

Nicolò Vaiana *, Salvatore Sessa, Luciano Rosati

Department of Structures for Engineering and Architecture, University of Naples Federico II, Via Claudio, 21, 80124 Napoli, Italy

ARTICLE INFO

Article history:
Received 5 January 2020
Received in revised form 16 April 2020
Accepted 15 May 2020
Available online xxxx

Keywords:
Asymmetric mechanical hysteresis
Rate-independent model
Accuracy
Computational efficiency

ABSTRACT

We extend a recently developed class of uniaxial symmetric rate-independent models to simulate complex asymmetric mechanical hysteresis phenomena. The main features of the novel formulation, that allows for the evaluation of the generalized force by solving a scalar equation and employing only one history variable, are illustrated by developing two specific instances of the class, namely the Asymmetric Bilinear and Exponential Models. The former is presented to better illustrate the meaning of the quantities entering the proposed formulation; the latter, representing a more sophisticated model able to simulate a wide range of asymmetric hysteretic behaviors, is illustrated to demonstrate the potentialities of the class in terms of accuracy and computational efficiency. To validate the Asymmetric Exponential Model, some experimental hysteresis loops, selected from the literature, are numerically simulated. Then, some nonlinear time history analyses are performed on a single degree of freedom mechanical system and the numerical results obtained by means of the proposed model are compared to those obtained by employing a modified version of the Bouc-Wen model.

1. Introduction

Hysteresis is a widespread complex phenomenon observed in many areas of science and engineering, especially in magnetics and mechanics. Hysteresis occurring in magnetic systems and materials is denominated *magnetic hysteresis*, whereas the one observed in mechanical systems and materials is referred to as *mechanical hysteresis* [37].

The hysteretic behavior of mechanical systems and materials, of specific interest in this work, is intrinsically nonlinear since their output not only depends on the current value of the input but also on its past history [6]. Specifically, such systems and materials exhibit a *rate-independent* hysteretic behavior, typically resulting from plastic deformation mechanisms and/or friction [24], when the generalized force (generalized displacement) does not depend on the rate of variation of the applied generalized displacement (generalized force) [9]. Notice that generalized forces include forces, moments, and stresses, whereas generalized displacements include displacements, rotations, and strains.

In particular, if one imposes a generalized cyclic displacement, the resulting generalized force, representing the output variable, traces a hysteresis loop in the generalized force-displacement plane. During a generic loading (unloading) phase, a typical hysteresis loop may be described by two types of curves, namely a generic loading (unloading) curve and an upper (a lower) bound [33,34].

* Corresponding author.
E-mail address: nicolo.vaiana@unina.it (N. Vaiana).

https://doi.org/10.1016/j.ymssp.2020.106984
0888-3270/

According to the type of shape characterizing typical generalized force-displacement hysteresis loops, it is possible to distinguish between *symmetric* and *asymmetric* mechanical hysteresis phenomena. In the former case, a typical hysteresis loop may be described by a loading curve (upper bound) having the same shape of the unloading curve (lower bound). On the contrary, in the latter case, a typical hysteresis loop may be described by generic loading and unloading curves and/or upper and lower bounds having different shapes.

Several uniaxial phenomenological models have been proposed in the literature for reproducing the complex asymmetric hysteresis phenomena occurring in rate-independent mechanical systems and materials. Looking at the type of the equation to adopt for the evaluation of the output variable, such models may be classified into four categories: algebraic, transcendental, differential, and integral models.

Differential models are the most employed ones to simulate asymmetric hysteresis phenomena. In particular, many of them represent an improved version of the original Bouc-Wen model, one of the most widespread symmetric models available in the literature [7,39,40]. In this differential model, belonging to the more general Duhem class of operators [12], the expression of the generalized force is computed by summing two components, that is, a linear elastic force and a rate-independent hysteretic force. The former is a function of the generalized displacement, whereas the latter is a function of a generalized hysteretic variable evaluated by solving a first-order nonlinear ordinary differential equation.

The above-described existing asymmetric differential models may be further classified into two groups: models formulated by modifying the expression of the generalized force and models obtained by modifying the differential equation required to compute the generalized hysteretic variable. Specifically, in the differential models belonging to the first group, the generalized force is evaluated by summing a nonlinear elastic component, instead of a linear elastic one, and a hysteretic component premultiplied by a modulating function. Among these models, those formulated by Ref. [4,8,23], specifically developed to simulate the asymmetric hysteretic behavior displayed by wire rope isolators along their axial direction, represent the most popular ones. Such asymmetric models require, respectively, a set of fifteen, nine, and eleven parameters having no clear mechanical or graphical meaning; they differ both for the expressions proposed for the nonlinear elastic force and for the modulating function.

In the differential models belonging to the second group, in which the generalized force is computed by summing a linear elastic component and a hysteretic one, as in the original Bouc-Wen model, the generalized hysteretic variable is evaluated by solving a modified version of the first-order nonlinear ordinary differential equation. Specifically, Ref. [10] as well as Ref. [38] have modified such a differential equation by adding additional terms in order to obtain hysteresis loops characterized not only by asymmetric peak forces but also by loading and unloading curves with different shapes. These asymmetric hysteretic behaviors are typical of some metals, polymers, shape memory alloys, and reinforced-concrete or steel beam-column connections. The former (latter) model requires eight (seven) parameters with not clear mechanical or graphical significance. In 2006, Ref. [31] proposed a generalized Bouc-Wen model, also formulated by adding additional terms in the first-order nonlinear ordinary differential equation. This model, based on a set of ten parameters having no clear mechanical or graphical meaning, allows for the simulation of highly asymmetric hysteresis loops typical of some flexible connectors used in electrical substations.

Unfortunately, these existing asymmetric differential models have two major disadvantages. First of all, they are computationally inefficient since the first-order nonlinear ordinary differential equation, required to compute the generalized hysteretic variable, needs to be numerically solved by means of multi-steps [25] or Runge–Kutta methods [27] for each time step of a nonlinear dynamic analysis. Furthermore, they are based on a relatively large number of model parameters having no clear mechanical or graphical significance; this aspect not only makes necessary the use of quite sophisticated parameters identification procedures but it also makes complicated their use in practical applications.

In this paper we present an enhanced formulation of a class of uniaxial phenomenological models, recently developed by Ref. [33], to simulate complex asymmetric hysteresis phenomena typical of several rate-independent mechanical systems and materials. One of the advantages offered by such a general formulation, that assumes the generalized force (generalized displacement) as output (input) variable, is the possibility of developing asymmetric models not requiring the numerical solution of a differential equation to compute the generalized force. This aspect allows for a significant reduction of the typically high computational times characterizing nonlinear time history analyses performed by using existing asymmetric differential models. Furthermore, by using the general relations of such a formulation, one may develop novel asymmetric models that are not only based on a small number of parameters having a clear graphical significance, thus simplifying the parameters identification procedure and allowing their use in practice, but that also require a simple implementation algorithm.

The present paper is structured into three parts. In the first part (Section 2), we shortly describe rate-independent mechanical systems and materials having asymmetric hysteretic behavior, giving particular emphasis on the description of their typical generalized force–displacement hysteresis loops.

In the second part (Sections 3 and 4), we first illustrate the proposed enhanced formulation of the class of models; then, to better describe its properties, we develop two specific instances of the proposed class, namely the Asymmetric Bilinear Model and Asymmetric Exponential Model. The former is presented to clearly explain the meaning of the adopted quantities, whereas the latter is illustrated to show the potentialities of the class in terms of accuracy and computational efficiency.

Finally, in the third part (Section 5), we validate the more elaborate Asymmetric Exponential Model, capable of simulating a large spectrum of asymmetric mechanical hysteresis phenomena, by means of experimental and numerical verifications.

Please cite this article as: N. Vaiana, S. Sessa and L. Rosati, A generalized class of uniaxial rate-independent models for simulating asymmetric mechanical hysteresis phenomena, Mechanical Systems and Signal Processing, https://doi.org/10.1016/j.ymssp.2020.106984

2. Mechanical systems and materials exhibiting an asymmetric hysteretic behavior

In the field of aerospace, civil, and mechanical engineering there exist several examples of mechanical systems and materials displaying complex rate-independent hysteretic behaviors. The term *rate-independent* means that the output variable of such systems and materials does not depend on the first time derivative of the input variable [9], this last one being represented either by a generalized force f or a generalized displacement u.

In particular, mechanical systems and materials display a *kinematic hardening* (*softening*) rate-independent hysteretic behavior if the generalized force f increases (decreases) with the generalized displacement u and the vertical distance between the two bounds limiting their hysteresis loops does not change during the nonlinear response.

Looking at the shape of the generalized force-displacement hysteresis loops, generally displayed by the above-described mechanical systems and materials, it is possible to distinguish between *symmetric* and *asymmetric* hysteresis loops. The former are characterized by a generic loading curve and an upper bound having, respectively, the same shape of the unloading curve and lower bound; on the contrary, the latter are defined by generic loading and unloading curves and/or upper and lower bounds with different shapes.

Depending on the types and analytical properties of the upper and lower bounds, asymmetric hysteresis loops, of particular interest in this work, may be classified into four main categories, as illustrated in Figs. 1 and 2. Specifically, Fig. 1a (1b) shows a typical asymmetric hysteresis loop limited by two parallel (non-parallel) straight lines, whereas Fig. 2a (2b) presents a typical asymmetric hysteresis loop delimited by two curves having no (one) inflection point. Such a classification has been carried out after a very careful examination of an extensive number of experimental asymmetric hysteresis loops available in the engineering literature; some of them are quoted in the next two paragraphs.

Some examples of systems and materials whose nonlinear response is characterized by asymmetric hysteresis loops bounded by two straight lines, as the ones illustrated in Fig. 1, are beam-column connections of steel moment-resisting frame structures [17,26,30], steel reinforcing bars used in beam and column elements of reinforced-concrete frame structures [16,22,28], and some types of spring connectors typically incorporated in electrical bus conductors to accommodate thermal effects [13].

Furthermore, examples of mechanical systems and materials with asymmetric hysteresis loops limited by two curves, as the ones shown in Fig. 2, are shape memory alloy springs, adopted to reduce the oscillations of flat plates due to flutter instability [21], martensitic nickel-titanium shape memory alloy bars [2,18], austenitic nickel-titanium shape memory alloy wires [11], metallic alloys [5] as well as actuators [1,41,43]. Additional examples are some flexible connectors [13], some rubber-like materials [19,20,42], and the class of wire rope springs, including helical, arch, and spherical wire rope devices, adopted not only for reducing the vibrations of bearings employed in rocket engines [32], but also for the seismic protection of equipment [8] and lightweight structures [36], and for the seismic retrofit of HV ceramic circuit breakers [3,4].

3. Proposed class of asymmetric models

The development of computationally efficient hysteretic models, able to reproduce generalized force–displacement hysteresis loops having a highly asymmetric shape and, at the same time, based on few parameters describing specific graphical properties of the hysteresis loops, represents such a challenging task.

In this section we present an enhanced formulation of a class of rate-independent models, recently developed by Vaiana et al. [33], able to reproduce the complex asymmetric hysteresis phenomena characterizing the behavior of several mechanical systems and materials. In particular, we first illustrate the adopted nomenclature and the novel general form proposed

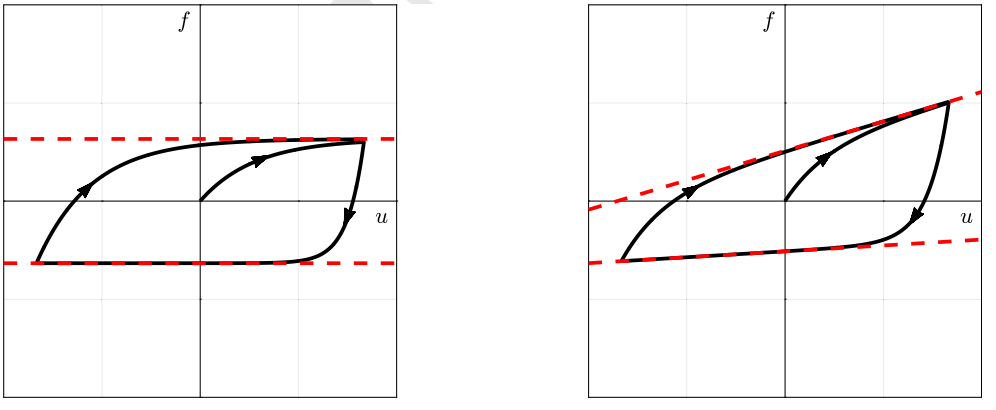

Fig. 1. Typical asymmetric hysteresis loop limited by two parallel (a) and non-parallel (b) straight lines.

Please cite this article as: N. Vaiana, S. Sessa and L. Rosati, A generalized class of uniaxial rate-independent models for simulating asymmetric mechanical hysteresis phenomena, Mechanical Systems and Signal Processing, https://doi.org/10.1016/j.ymssp.2020.106984

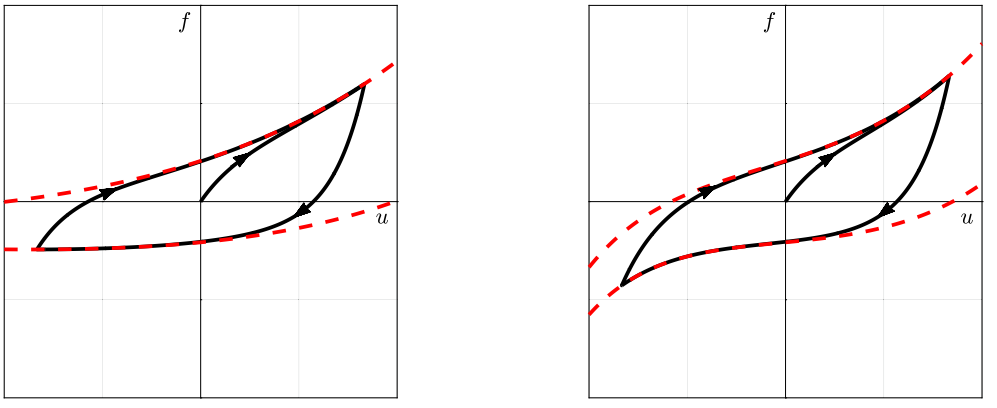

(a) (b)

Fig. 2. Typical asymmetric hysteresis loop limited by two curves without (a) and with (b) inflection point.

for the generalized tangent stiffness k_t; then, we derive the general expressions of the generalized force f and of the history variable u_j, and, finally, we obtain two general expressions relating the parameters f_0 and u_0.

3.1. Preliminaries

Fig. 3a (3b) shows a typical asymmetric hysteresis loop limited by two straight lines (curves), described by means of four different curves, namely the upper c_u and lower c_l limiting curves and the generic loading c^+ and unloading c^- curves.

The upper (lower) limiting curve c_u (c_l) intersects the vertical axis at a point with coordinates 0 and f_0^+ (0 and $-f_0^-$). By supposing that such limiting curves are not affected by cyclic loading phenomena, the distance between them, evaluated along the vertical axis at a generic point having abscissa u, remains constant.

The generic loading curve c^+, describing the response when the sign of the generalized velocity $\dot{u}$ is positive, intersects the lower (upper) limiting curve at a generic point having abscissa u_i^+ (u_j^+), with $u_i^+ = u_j^+ - 2u_0^+$; similarly, the generic unloading curve c^-, describing the response when the sign of the velocity $\dot{u}$ is negative, intersects the upper (lower) limiting curve at a generic point having abscissa u_i^- (u_j^-), with $u_i^- = u_j^- + 2u_0^-$.

3.2. Generalized tangent stiffness

The asymmetric hysteresis loops in Fig. 3 are typically modeled in the literature [14] by adopting two parallel uniaxial springs: an elastic one, characterized by a generalized force f_e and a generalized tangent stiffness $k_e = df_e/du, u$ being the

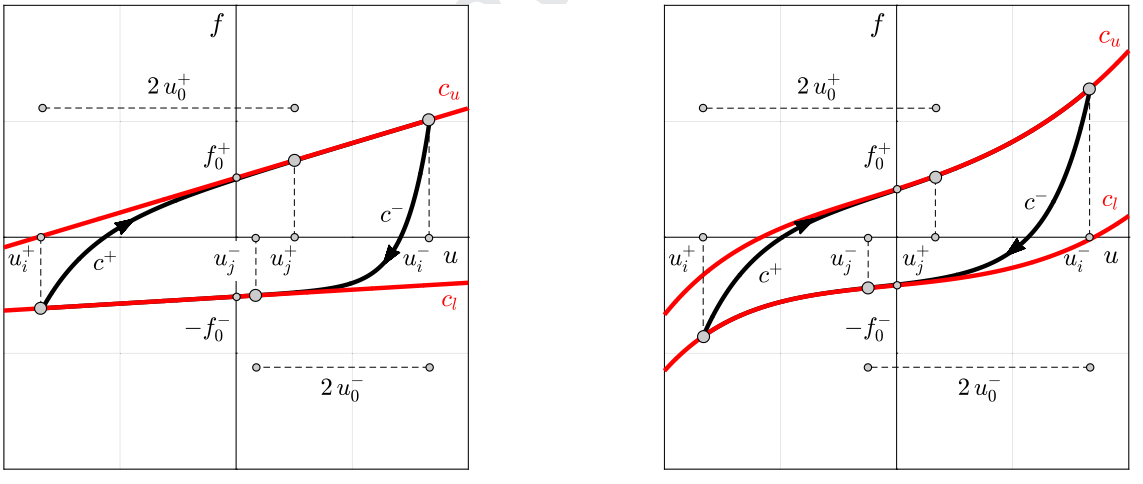

(a) (b)

Fig. 3. Curves c_u, c_l, c^+, and c^- for an asymmetric hysteresis loop limited by two straight lines (a) or curves (b).

Please cite this article as: N. Vaiana, S. Sessa and L. Rosati, A generalized class of uniaxial rate-independent models for simulating asymmetric mechanical hysteresis phenomena, Mechanical Systems and Signal Processing, https://doi.org/10.1016/j.ymssp.2020.106984

generalized displacement, and a hysteretic one, characterized by a generalized force $\hat{f}_h$ and a generalized tangent stiffness $\hat{k}_h = d\hat{f}_h/du$. Accordingly, for modeling purposes, we assume that a typical asymmetric hysteresis loop, as the one illustrated in Fig. 4a, can be decomposed as the sum of two different functions, namely f_e and $\hat{f}_h$; the former, shown in Fig. 4b, is a single-valued function having zero value at $u = 0$, that is, $f_e(0) = 0$, whereas the latter, shown in Fig. 4c, is obtained in turn by premultiplying a multi-valued function f_h by a single-valued one ψ having unit value at $u = 0$, that is, $\psi(0) = 1$. The conditions $f_e(0) = 0$ and $\psi(0) = 1$ ensure that the upper (lower) limiting curve of a generalized force–displacement hysteresis loop intersects the vertical axis at $(0, f_0^+)$ $((0, -f_0^-))$, as shown in Fig. 3.

As an example, in order to obtain a function $\hat{f}_h = \psi f_h$ characterized by two non-parallel limiting curves (Fig. 5a), we may multiply a positive convex and differentiable function ψ (Fig. 5b) by a function f_h having two parallel limiting straight lines (Fig. 5c). Since the function ψ allows us to modify the shape of the bounds characterizing function f_h, as clearly illustrated in Fig. 5, we call ψ *shaping function*.

Coherently with the previous assumptions, the general form of the generalized tangent stiffness k_t is:

$$k_t(u, u_j) = k_e(u) + \hat{k}_h(u, u_j), \tag{1}$$

with:

$$\hat{k}_h(u, u_j) = \psi(u) k_h(u, u_j) + \frac{d\psi(u)}{du} \int k_h(u, u_j) du, \tag{2}$$

where $k_e(u)$ and $\psi(u)$ are functions of the generalized displacement u, whereas $k_h(u, u_j)$ is a function of both the generalized displacement u and the history variable u_j; such a variable is represented by u_j^+ (u_j^-) in the generic loading (unloading) case or, in other words, when the generalized velocity $\dot{u}$ is positive (negative).

As explained in details in Ref. [33], $k_h(u, u_j)$ is an arbitrary function having initial value k_a^+ (k_a^-) on $[u_j^+ - 2u_0^+, u_j^+[$ $(]u_j^-, u_j^- + 2u_0^-])$, when $\dot{u} > 0$ $(\dot{u} < 0)$, whereas it is constant and equal to k_b^+ (k_b^-) on $]u_j^+, \infty)$ $((-\infty, u_j^-[)$, when $\dot{u} > 0$ $(\dot{u} < 0)$.

Note that setting $\psi(u) = 1$ in Eq. (2), Eq. (1) becomes:

$$k_t(u, u_j) = k_e(u) + k_h(u, u_j), \tag{3}$$

which represents the general form of k_t presented in the original formulation developed in Ref. [33].

3.3. Generalized force

The generalized force f can be evaluated by adopting the expressions of the four curves that characterize a typical asymmetric hysteresis loop, that is, the upper c_u and lower c_l limiting curves and the generic loading c^+ and unloading c^- curves; specifically, as shown in Fig. 3, in the generic loading (unloading) case, $f = c^+$ $(f = c^-)$ when $u_i^+ \leqslant u < u_j^+$ $(u_j^- < u \leqslant u_i^-)$, and $f = c_u$ $(f = c_l)$ when $u > u_j^+$ $(u < u_j^-)$. Thus, in the following subsection, we derive the general expressions of such curves by integrating the novel general expression proposed for k_t.

3.3.1. Upper limiting curve

To derive the expression of c_u, we integrate Eq. (1) by obtaining:

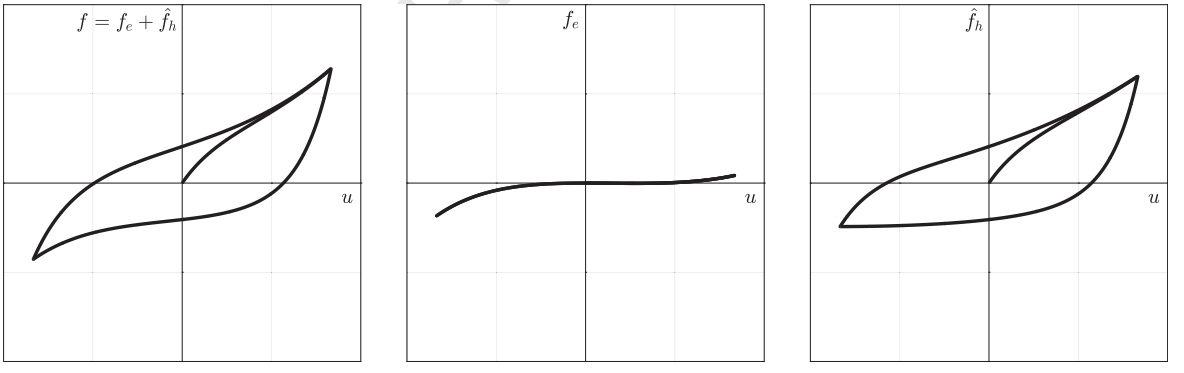

Fig. 4. Typical asymmetric hysteresis loop (a) obtained by summing functions f_e (b) and $\hat{f}_h$ (c).

Please cite this article as: N. Vaiana, S. Sessa and L. Rosati, A generalized class of uniaxial rate-independent models for simulating asymmetric mechanical hysteresis phenomena, Mechanical Systems and Signal Processing, https://doi.org/10.1016/j.ymssp.2020.106984

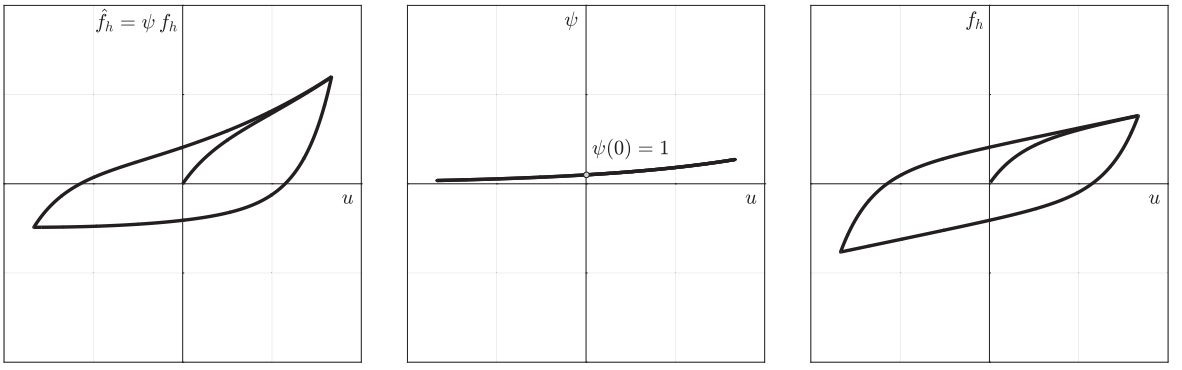

Fig. 5. Function $\hat{f}_h$ (a) obtained by multiplying the shaping function ψ (b) by function f_h(c).

$$c_u\left(u, u_j^+\right) = \int k_e(u)du + \int \psi(u) k_h\left(u, u_j^+\right)du + \int \frac{d\psi(u)}{du}\left(\int k_h\left(u, u_j^+\right)du\right)du, \tag{4}$$

which, upon integrating by parts the second addend, can be also written as:

$$c_u\left(u, u_j^+\right) = \int k_e(u)du + \psi(u)\int k_h\left(u, u_j^+\right)du. \tag{5}$$

Since the function c_u comes into play when $u > u_j^+$, we can set $k_h(u, u_j^+) = k_b^+$. Hence, Eq. (5) becomes:

$$c_u(u) = f_e(u) + C_e + \psi(u)\left(k_b^+ u + C_u\right), \tag{6}$$

where:

$$f_e(u) = \int k_e(u)du. \tag{7}$$

To determine the integration constant C_e, we impose $c_u(0) = 0$ when $\psi(u) = 0$; thus, having assumed $f_e(0) = 0$, we obtain:

$$C_e = 0. \tag{8}$$

As regards the evaluation of C_u, we impose that the curve c_u intersects the vertical axis at a point with coordinates 0 and f_0^+:

$$f_e(0) + \psi(0)C_u = f_0^+, \tag{9}$$

from which, having assumed $f_e(0) = 0$ and $\psi(0) = 1$ when $\psi(u) \neq 0$, we obtain:

$$C_u = f_0^+. \tag{10}$$

Thus, the general expression of $c_u(u)$ is:

$$c_u(u) = f_e(u) + \psi(u)\left(k_b^+ u + f_0^+\right). \tag{11}$$

3.3.2. Lower limiting curve

Similarly to c_u, the expression of c_l can be determined by integrating Eq. (1):

$$c_l\left(u, u_j^-\right) = \int k_e(u)du + \int \psi(u) k_h\left(u, u_j^-\right)du + \int \frac{d\psi(u)}{du}\left(\int k_h\left(u, u_j^-\right)du\right)du, \tag{12}$$

and by applying the integration by parts to the second addend of Eq. (12), thus obtaining:

$$c_l\left(u, u_j^-\right) = \int k_e(u)du + \psi(u)\int k_h\left(u, u_j^-\right)du. \tag{13}$$

Being interested in expressing the function c_l, we assume $u < u_j^-$ so that $k_h(u, u_j^-) = k_b^-$ and Eq. (13) can be written as:

$$c_l(u) = f_e(u) + C_e + \psi(u)\left(k_b^- u + C_l\right), \tag{14}$$

where $f_e(u)$ and C_e are given by Eqs. (7) and (8), respectively. The integration constant C_l can be derived by imposing that the curve c_l intersects the vertical axis at a point with coordinates 0 and $-f_0^-$:

$$f_e(0) + \psi(0) C_l = -f_0^- . \tag{15}$$

Since we have assumed $f_e(0) = 0$ and $\psi(0) = 1$ when $\psi(u) \neq 0$, Eq. (15) gives:

$$C_l = -f_0^- , \tag{16}$$

and, consequently, the general expression of $c_l(u)$ becomes:

$$c_l(u) = f_e(u) + \psi(u)\left(k_b^- u - f_0^-\right). \tag{17}$$

We note that the distance between the upper and lower limiting curves, evaluated along the vertical axis at a generic point with abscissa u, is equal to $\psi(u)[(k_b^+ - k_b^-)u + f_0^+ + f_0^-]$; in particular, such a distance becomes equal to $f_0^+ + f_0^-$ for $u = 0$, having assumed $\psi(0) = 1$.

3.3.3. Generic loading curve

To find the expression of c^+, we first integrate Eq. (1) to have:

$$c^+\left(u, u_j^+\right) = \int k_e(u)du + \int \psi(u) k_h\left(u, u_j^+\right)du + \int \frac{d\psi(u)}{du}\left(\int k_h\left(u, u_j^+\right)du\right)du, \tag{18}$$

and then we integrate by parts the second addend of Eq. (18) to get:

$$c^+\left(u, u_j^+\right) = \int k_e(u)du + \psi(u)\int k_h\left(u, u_j^+\right)du. \tag{19}$$

Such an equation can be equivalently rewritten as:

$$c^+\left(u, u_j^+\right) = f_e(u) + C_e + \psi(u)\left(f_h\left(u, u_j^+\right) + C^+\right), \tag{20}$$

where $f_e(u)$ and C_e are given by Eqs. (7) and (8), respectively, whereas $f_h(u, u_j^+)$ is computed as:

$$f_h\left(u, u_j^+\right) = \int k_h\left(u, u_j^+\right)du. \tag{21}$$

To evaluate the integration constant C^+, we impose that the curve c^+ intersects the upper limiting curve at $u = u_j^+$:

$$c^+\left(u_j^+, u_j^+\right) = c_u\left(u_j^+\right). \tag{22}$$

Hence, on account of Eq. (11), we have:

$$f_e\left(u_j^+\right) + \psi\left(u_j^+\right)\left(f_h\left(u_j^+, u_j^+\right) + C^+\right) = f_e\left(u_j^+\right) + \psi\left(u_j^+\right)\left(k_b^+ u_j^+ + f_0^+\right), \tag{23}$$

from which we obtain:

$$C^+ = k_b^+ u_j^+ + f_0^+ - f_h\left(u_j^+, u_j^+\right). \tag{24}$$

In conclusion, the general expression of c^+ is:

$$c^+\left(u, u_j^+\right) = f_e(u) + \psi(u)\left(f_h\left(u, u_j^+\right) + k_b^+ u_j^+ + f_0^+ - f_h\left(u_j^+, u_j^+\right)\right). \tag{25}$$

3.3.4. Generic unloading curve

Similarly to c^+, to derive the expression of c^-, Eq. (1) has to be integrated as follows:

$$c^-\left(u, u_j^-\right) = \int k_e(u)du + \int \psi(u) k_h\left(u, u_j^-\right)du + \int \frac{d\psi(u)}{du}\left(\int k_h\left(u, u_j^-\right)du\right)du, \tag{26}$$

and the second addend of Eq. (26) has to be integrated by parts, leading to:

$$c^-\left(u, u_j^-\right) = \int k_e(u)du + \psi(u)\int k_h\left(u, u_j^-\right)du. \tag{27}$$

The previous equation can be also written as:

$$c^-\left(u, u_j^-\right) = f_e(u) + C_e + \psi(u)\left(f_h\left(u, u_j^-\right) + C^-\right), \tag{28}$$

where $f_e(u)$ and C_e are evaluated by using Eqs. (7) and (8), respectively, whereas $f_h(u, u_j^-)$ is given by:

$$f_h\left(u, u_j^-\right) = \int k_h\left(u, u_j^-\right)du. \tag{29}$$

Please cite this article as: N. Vaiana, S. Sessa and L. Rosati, A generalized class of uniaxial rate-independent models for simulating asymmetric mechanical hysteresis phenomena, Mechanical Systems and Signal Processing, https://doi.org/10.1016/j.ymssp.2020.106984

The determination of the integration constant C^- requires to impose that the curve c^- intersects the lower limiting curve at $u = u_j^-$:

$$c^-\left(u_j^-, u_j^-\right) = c_l\left(u_j^-\right). \tag{30}$$

Hence, on account of Eq. (17), we get:

$$f_e\left(u_j^-\right) + \psi\left(u_j^-\right)\left(f_h\left(u_j^-, u_j^-\right) + C^-\right) = f_e\left(u_j^-\right) + \psi\left(u_j^-\right)\left(k_b^- u_j^- - f_0^-\right), \tag{31}$$

from which we have:

$$C^- = k_b^- u_j^- - f_0^- - f_h\left(u_j^-, u_j^-\right). \tag{32}$$

In conclusion, the general expression of c^- is:

$$c^-\left(u, u_j^-\right) = f_e(u) + \psi(u)\left(f_h\left(u, u_j^-\right) + k_b^- u_j^- - f_0^- - f_h\left(u_j^-, u_j^-\right)\right). \tag{33}$$

3.4. History variable

The generalized displacement u_j^+ (u_j^-), required for the evaluation of f during a generic loading (unloading) phase, represents the abscissa of the intersection point of a generic loading (unloading) curve and the upper (lower) limiting curve, as illustrated in Fig. 6. Since the quantity u_j^+ (u_j^-) is constant during an entire loading (unloading) phase, to increase the computational efficiency of the proposed formulation, we suggest to compute such a value only for the initial point $P : (u_P, f_P)$ of the generic loading (unloading) curve and to store it until the end of the loading (unloading) phase. This is the reason why such a generalized displacement is referred to as *history variable*.

In the following, we derive the general expression of u_j^+ (u_j^-) for a generic initial point P of c^+ (c^-) that lies between the two limiting curves.

3.4.1. Evaluation of u_j^+

To determine the expression of u_j^+, we impose that the generic loading curve c^+, given by Eq. (25), passes through the point $P : (u_P, f_P)$ by obtaining:

$$c^+\left(u_P, u_j^+\right) = f_P, \tag{34}$$

that gives:

$$f_e(u_P) + \psi(u_P)\left(f_h\left(u_P, u_j^+\right) + k_b^+ u_j^+ + f_0^+ - f_h\left(u_j^+, u_j^+\right)\right) = f_P, \tag{35}$$

from which we can evaluate u_j^+.

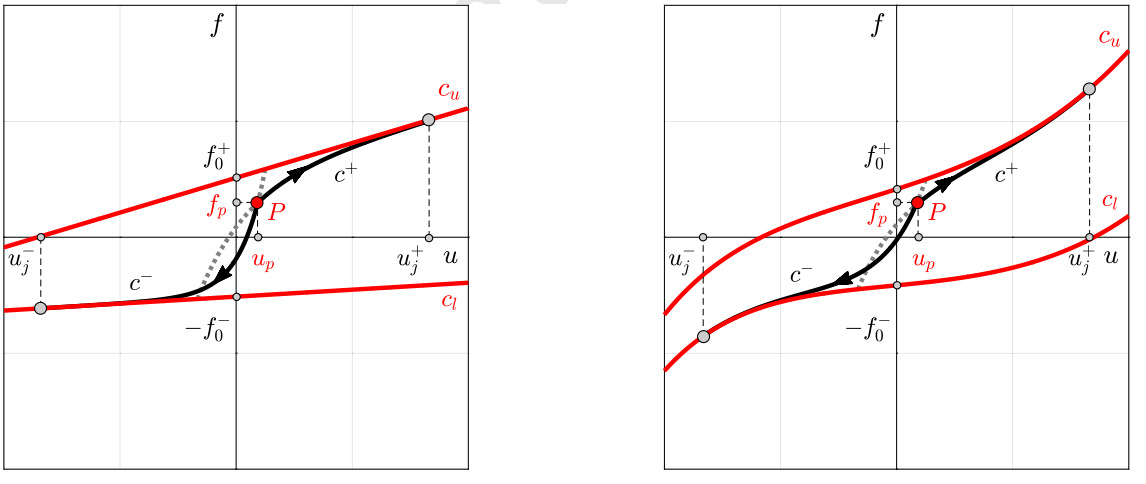

Fig. 6. Evaluation of the history variable u_j in the case of an asymmetric hysteresis loop limited by two straight lines (a) or curves (b).

Please cite this article as: N. Vaiana, S. Sessa and L. Rosati, A generalized class of uniaxial rate-independent models for simulating asymmetric mechanical hysteresis phenomena, Mechanical Systems and Signal Processing, https://doi.org/10.1016/j.ymssp.2020.106984

3.4.2. Evaluation of u_j^-

Similarly, we derive the expression of u_j^- by imposing that the generic unloading curve c^-, given by Eq. (33), passes through the point $P:(u_P, f_P)$:

$$c^-\left(u_P, u_j^-\right) = f_P, \tag{36}$$

so that we obtain:

$$f_e(u_P) + \psi(u_P)\left(f_h\left(u_P, u_j^-\right) + k_b^- u_j^- - f_0^- - f_h\left(u_j^-, u_j^-\right)\right) = f_P, \tag{37}$$

from which we can compute u_j^-.

Note that we can compute u_j^+ (u_j^-), by adopting Eq. (35) (Eq. (37)), either in closed form or numerically depending on the expression of the function $f_h(u, u_j^+)$ ($f_h(u, u_j^-)$) that is obtained by integrating the expression selected for $k_h(u, u_j^+)$ ($k_h(u, u_j^-)$).

3.5. Parameters

For the ensuing developments, it is crucial to derive a general expression relating the parameters f_0^+, f_0^-, and u_0^+. To this end, we impose that c^+ intersects the lower limiting curve at $u = u_i^+$, where $u_i^+ = u_j^+ - 2u_0^+$:

$$c^+\left(u_j^+ - 2u_0^+, u_j^+\right) = c_l\left(u_j^+ - 2u_0^+\right). \tag{38}$$

On account of Eqs. (17) and (25), the previous equation becomes:

$$\begin{aligned} &f_e\left(u_j^+ - 2u_0^+\right) + \psi\left(u_j^+ - 2u_0^+\right)\left(f_h\left(u_j^+ - 2u_0^+, u_j^+\right) + k_b^+ u_j^+ + f_0^+ - f_h\left(u_j^+, u_j^+\right)\right) \\ &\quad = f_e\left(u_j^+ - 2u_0^+\right) + \psi\left(u_j^+ - 2u_0^+\right)\left[k_b^-\left(u_j^+ - 2u_0^+\right) - f_0^-\right], \end{aligned} \tag{39}$$

which gives:

$$f_h\left(u_j^+ - 2u_0^+, u_j^+\right) + (k_b^+ - k_b^-)u_j^+ + 2k_b^- u_0^+ + f_0^+ + f_0^- - f_h\left(u_j^+, u_j^+\right) = 0. \tag{40}$$

Similarly, to find a general expression relating the parameters f_0^+, f_0^-, and u_0^-, we impose that c^- intersects the upper limiting curve at $u = u_i^-$, where $u_i^- = u_j^- + 2u_0^-$:

$$c^-\left(u_j^- + 2u_0^-, u_j^-\right) = c_u\left(u_j^- + 2u_0^-\right). \tag{41}$$

By using Eqs. (11) and (33), the previous equation can be rewritten as:

$$\begin{aligned} &f_e\left(u_j^- + 2u_0^-\right) + \psi\left(u_j^- + 2u_0^-\right)\left(f_h\left(u_j^- + 2u_0^-, u_j^-\right) + k_b^- u_j^- - f_0^- - f_h\left(u_j^-, u_j^-\right)\right) \\ &\quad = f_e\left(u_j^- + 2u_0^-\right) + \psi\left(u_j^- + 2u_0^-\right)\left[k_b^+\left(u_j^- + 2u_0^-\right) + f_0^+\right], \end{aligned} \tag{42}$$

thus obtaining:

$$f_h\left(u_j^- + 2u_0^-, u_j^-\right) - (k_b^+ - k_b^-)u_j^- - 2k_b^+ u_0^- - f_0^+ - f_0^- - f_h\left(u_j^-, u_j^-\right) = 0. \tag{43}$$

It will be shown in subSection 4.1 that once the values of the parameters f_0^+ and f_0^- have been set, u_0^+ (u_0^-) can be obtained from Eq. (40) (Eq. (43)) either in closed form or numerically according to the type of function $f_h(u, u_j^+)$ ($f_h(u, u_j^-)$) that is obtained by integrating the expression selected for $k_h(u, u_j^+)$ ($k_h(u, u_j^-)$), similarly to what has been shown for the evaluation of u_j^+ (u_j^-).

Furthermore, it will be shown in subsection 4.2 that, setting $k_b^+ = k_b^- = k_b$, $u_0^+ = u_0^- = u_0$, and imposing that $f_0^- = cf_0^+$ ($f_0^+ = cf_0^-$), c being a positive real constant, we may adopt Eq. (40) or, equivalently, Eq. (43) to evaluate f_0^+ (f_0^-), either in closed form or numerically according to the type of function f_h we obtain by integrating the expression selected for k_h.

4. Two instances of the class: The Asymmetric Bilinear and Exponential Models

In this section we develop two specific instances of the proposed generalized class, namely the Asymmetric Bilinear Model and the Asymmetric Exponential Model, to better explain the procedure that allows for the development of new models by using the general relations described in Section 3. In particular, we first present the Asymmetric Bilinear Model to easily describe the meaning of the adopted quantities; then, we present the Asymmetric Exponential Model to illustrate the potentialities of such a class in accurately reproducing complex asymmetric hysteresis phenomena.

Please cite this article as: N. Vaiana, S. Sessa and L. Rosati, A generalized class of uniaxial rate-independent models for simulating asymmetric mechanical hysteresis phenomena, Mechanical Systems and Signal Processing, https://doi.org/10.1016/j.ymssp.2020.106984

4.1. Asymmetric Bilinear Model

We describe the model by defining, in turn, the generalized tangent stiffness, the generalized force, the history variable, the internal model parameter, and by illustrating the types of hysteresis loop shape that can be simulated.

4.1.1. Generalized tangent stiffness

The adopted generalized tangent stiffness functions are:

$$k_e(u) = 0 \quad \text{on } (-\infty, \infty), \tag{44}$$

$$k_h(u, u_j^+) = \begin{cases} k_a^+ & \text{on } \left[u_j^+ - 2u_0^+, u_j^+\right[\quad (45a) \\ k_b^+ & \text{on } \left]u_j^+, \infty\right), \quad (45b) \end{cases}$$

$$k_h(u, u_j^-) = \begin{cases} k_a^- & \text{on } \left]u_j^-, u_j^- + 2u_0^-\right] \quad (46a) \\ k_b^- & \text{on } \left(-\infty, u_j^-\right[, \quad (46b) \end{cases}$$

whereas the selected shaping function is:

$$\psi(u) = 1 \quad \text{on } (-\infty, \infty), \tag{47}$$

where $k_a^+,\ k_b^+,\ k_a^-,\ k_b^-$ represent, together with f_0^+ and f_0^- introduced in Section 3, the six model parameters to be identified on the basis of experimental or numerical tests results; in particular, such parameters satisfy the following conditions: $k_a^+ > k_b^+,\ k_a^+ > k_b^-,\ k_a^+ > 0,\ f_0^+ > 0,\ k_a^- > k_b^-,\ k_a^- > k_b^+,\ k_a^- > 0$, and $f_0^- > 0$.

The function k_h, illustrated in Fig. 7a (7b) for the generic loading (unloading) case, is discontinuous at u_j^+ (u_j^-); thus, in such a model, the curves c^+ and c_u (c^- and c_l) have two different tangents at u_j^+ (u_j^-), as shown in the next subsections.

Note that assuming $k_a^+ = k_a^-$ and $k_b^+ = k_b^-$, we obtain the generalized tangent stiffness functions adopted in the Bilinear Model described in Ref. [33].

4.1.2. Generalized force

We now derive the expressions of the upper (lower) limiting curve c_u (c_l) and of the generic loading (unloading) curve c^+ (c^-) required for the evaluation of the generalized force f during the generic loading (unloading) phase.

Upper (Lower) Limiting Curve

According to the definition (7) and to the assumption (44), we have:

$$f_e(u) = 0. \tag{48}$$

Hence, taking into account (47) and (48), Eq. (11) becomes:

$$c_u(u) = k_b^+ u + f_0^+, \tag{49}$$

whereas Eq. (17) yields:

$$c_l(u) = k_b^- u - f_0^-. \tag{50}$$

Generic Loading (Unloading) Curve

Because of the assumption (45a), Eq. (21) specializes to:

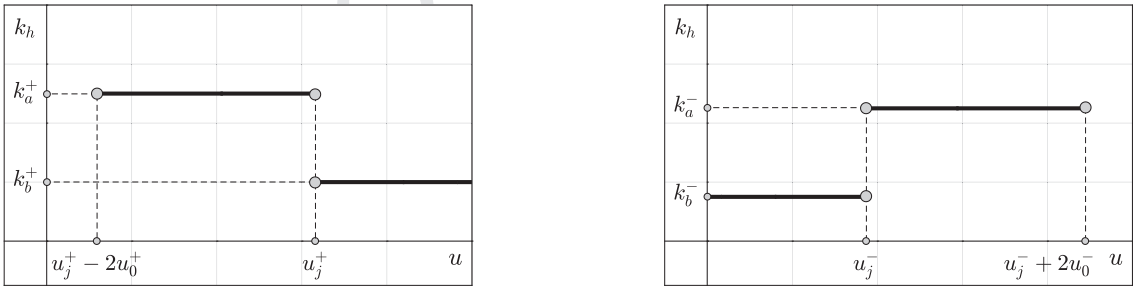

Fig. 7. Graph of the function k_h for the generic loading (a) and unloading (b) case (Asymmetric Bilinear Model).

Please cite this article as: N. Vaiana, S. Sessa and L. Rosati, A generalized class of uniaxial rate-independent models for simulating asymmetric mechanical hysteresis phenomena, Mechanical Systems and Signal Processing, https://doi.org/10.1016/j.ymssp.2020.106984

$$f_h(u,u_j^+) = k_a^+ u, \tag{51}$$

so that, recalling (47) and (48), Eq. (25) yields:

$$c^+(u,u_j^+) = k_a^+(u-u_j^+) + k_b^+ u_j^+ + f_0^+. \tag{52}$$

Similarly, on account of the assumption (46a), Eq. (29) becomes:

$$f_h(u,u_j^-) = k_a^- u. \tag{53}$$

Hence, taking into account (47) and (48), Eq. (33) yields:

$$c^-(u,u_j^-) = k_a^-(u-u_j^-) + k_b^- u_j^- - f_0^-. \tag{54}$$

4.1.3. History variable

Invoking (48) and (51), and taking into account the assumption (47), Eq. (35) becomes:

$$k_a^+ u_P + k_b^+ u_j^+ + f_0^+ - k_a^+ u_j^+ = f_P, \tag{55}$$

from which we obtain the expression of the history variable for the generic loading case:

$$u_j^+ = \frac{k_a^+ u_P + f_0^+ - f_P}{k_a^+ - k_b^+}. \tag{56}$$

Similarly, using (48) and (53), and taking into account (47), Eq. (37) specializes to:

$$k_a^- u_P + k_b^- u_j^- - f_0^- - k_a^- u_j^- = f_P, \tag{57}$$

from which we obtain the expression of the history variable for the generic unloading case:

$$u_j^- = \frac{k_a^- u_P - f_0^- - f_P}{k_a^- - k_b^-}. \tag{58}$$

Note that Eq. (56) (Eq. (58)) may provide positive or negative values of u_j^+ (u_j^-) according to the coordinates of the initial point $P:(u_P,f_P)$ of c^+ (c^-).

4.1.4. Expression of u_0^+ (u_0^-)

We determine the expression of u_0^+ (u_0^-), referred to as *internal model parameter* since it can be expressed as a function of the model parameters described in 4.1.1. In particular, to derive the expression of u_0^+, we use Eqs. (40) and (51) to get:

$$k_a^+\left(u_j^+ - 2u_0^+\right) + (k_b^+ - k_b^-)u_j^+ + 2k_b^- u_0^+ + f_0^+ + f_0^- - k_a^+ u_j^+ = 0, \tag{59}$$

from which we obtain:

$$u_0^+ = \frac{(k_b^+ - k_b^-)u_j^+ + f_0^+ + f_0^-}{2(k_a^+ - k_b^-)}. \tag{60}$$

Similarly, to find the expression of u_0^-, we use Eqs. (43) and (53) to obtain:

$$k_a^-\left(u_j^- + 2u_0^-\right) - (k_b^+ - k_b^-)u_j^- - 2k_b^+ u_0^- - f_0^+ - f_0^- - k_a^- u_j^- = 0, \tag{61}$$

from which we get:

$$u_0^- = \frac{(k_b^+ - k_b^-)u_j^- + f_0^+ + f_0^-}{2(k_a^- - k_b^+)}. \tag{62}$$

Note that, when $k_b^+ \neq k_b^-$, the parameter u_0^+ (u_0^-) is not constant since it depends on the history variable u_j^+ (u_j^-). On the contrary, when $k_b^+ = k_b^-$, Eq. (60) (Eq. (62)) provides a constant value of u_0^+ (u_0^-); such a value is positive being $k_a^+ > k_b^-$ ($k_a^- > k_b^+$) as well as $f_0^+ > 0$ and $f_0^- > 0$.

4.1.5. Hysteresis loop shapes

Fig. 8 illustrates two different asymmetric hysteresis loop shapes that can be obtained by means of the Asymmetric Bilinear Model. In particular, Fig. 8a presents a hysteresis loop bounded by two parallel straight lines, whereas Figs. 8b and 8c show hysteresis loops bounded by two non-parallel straight lines. Such hysteresis loops, typical of some hysteretic mechanical systems and materials [13,16,17,22,26,30], have been simulated by imposing a generalized sinusoidal displacement having unit amplitude and frequency and by using the six model parameters listed in Table 1.

Please cite this article as: N. Vaiana, S. Sessa and L. Rosati, A generalized class of uniaxial rate-independent models for simulating asymmetric mechanical hysteresis phenomena, Mechanical Systems and Signal Processing, https://doi.org/10.1016/j.ymssp.2020.106984

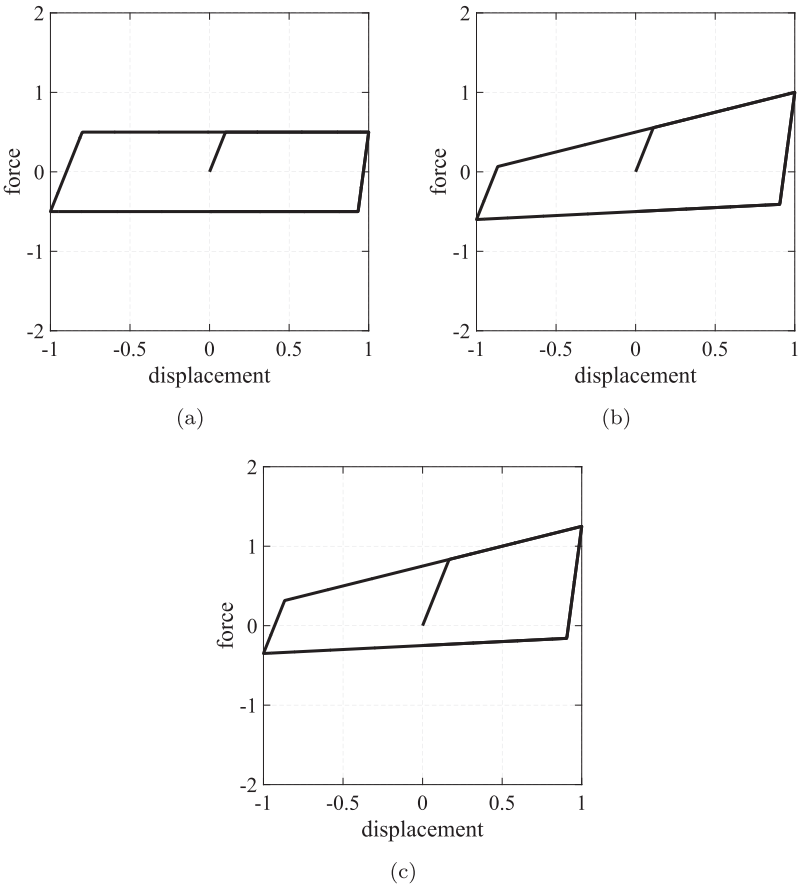

Fig. 8. Hysteresis loops simulated by using the Asymmetric Bilinear Model parameters given in Table 1.

Table 1
Asymmetric Bilinear Model parameters adopted for the hysteresis loops in Fig. 8.

	k_a^+	k_b^+	f_0^+	k_a^-	k_b^-	f_0^-
(a)	5.0	0.0	0.5	15.0	0.0	0.5
(b)	5.0	0.5	0.5	15.0	0.1	0.5
(c)	5.0	0.5	0.75	15.0	0.1	0.25

4.2. Asymmetric Exponential Model

As for the Asymmetric Bilinear Model, we define, in turn, the generalized tangent stiffness, the generalized force, the history variable, and the internal model parameter that characterize the Asymmetric Exponential Model; then we illustrate the types of hysteresis loop shape that the model can reproduce.

4.2.1. Generalized tangent stiffness

The adopted generalized tangent stiffness functions are:

$$k_e(u) = -(\beta_1 + \beta_2) + \beta_1 e^{\beta_1 u} + \beta_2 e^{-\beta_2 u} \quad \text{on } (-\infty, \infty), \tag{63}$$

$$k_h(u, u_j^+) = \begin{cases} k_b^+ + (k_a^+ - k_b^+) e^{-\alpha^+ \left(u - u_j^+ + 2u_0^+\right)} & \text{on } \left[u_j^+ - 2u_0^+, u_j^+\right[\quad (64a) \\ k_b^+ & \text{on } \left]u_j^+, \infty\right), \quad (64b) \end{cases}$$

$$k_h(u,u_j^-) = \begin{cases} k_b^- + (k_a^- - k_b^-)e^{-\alpha^-\left(-u+u_j^-+2u_0^-\right)} & \text{on } \left]u_j^-, u_j^- + 2u_0^-\right] \quad (65a) \\ k_b^- & \text{on } \left(-\infty, u_j^-\right[, \quad (65b) \end{cases}$$

whereas the selected shaping function is:

$$\psi(u) = e^{\gamma u} \qquad \text{on } (-\infty, \infty), \tag{66}$$

where k_a^+, k_b^+, α^+, u_0^+, k_a^-, k_b^-, α^-, u_0^-, β_1, β_2, and γ are the model parameters. To reduce the number of parameters, although without impairing the capability of the model to reproduce very complex hysteretic behaviors, we further assume:

$$k_a^+ = k_a^- = k_a, \quad k_b^+ = k_b^- = k_b, \quad \alpha^+ = \alpha^- = \alpha, \quad \text{and} \quad u_0^+ = u_0^- = u_0. \tag{67}$$

Hence, the set of model parameters, to be identified on the basis of experimental or numerical tests results, becomes $k_a, k_b, \alpha, u_0, \beta_1, \beta_2$, and γ; specifically, such parameters satisfy the following conditions: $k_a > k_b$, $k_a > 0$, $\alpha > 0$, $u_0 > 0$, $\beta_1 \geqslant 0$, $\beta_2 \geqslant 0$, whereas γ is real. The more general modeling capabilities that can be achieved by adopting the original eleven parameters of the model will be investigated in forthcoming papers.

As regards the parameters β_1 and β_2, they define the shape of function k_e, a convex function on $(-\infty, \infty)$ when $\beta_1 \geqslant 0$ and $\beta_2 > 0$ or when $\beta_1 > 0$ and $\beta_2 \geqslant 0$.

The parameters k_a, k_b, α, and u_0 characterize the function k_h. Such a function, illustrated in Fig. 9a (9b) for the generic loading (unloading) case, is a nonlinearly decreasing function, from k_a to $k_b + (k_a - k_b)e^{-2\alpha u_0}$ on $[u_j^+ - 2u_0, u_j^+[$ ($]u_j^-, u_j^- + 2u_0]$), when $\dot{u} > 0$ ($\dot{u} < 0$), and is equal to k_b on $]u_j^+, \infty)$ ($(-\infty, u_j^-[$), when $\dot{u} > 0$ ($\dot{u} < 0$). In particular, the parameter α defines the rate of variation of k_h from k_a to $k_b + (k_a - k_b)e^{-2\alpha u_0}$.

The parameter u_0 can be expressed as a function of k_a, k_b, and α, thus it is referred to as *internal model parameter*. To derive such an expression, we first observe that $k_h(u, u_j^+)$ ($k_h(u, u_j^-)$) is discontinuous at u_j^+ (u_j^-), as shown in Fig. 9a (9b). Hence, if we denote the difference between the two different stiffness values of $k_h(u, u_j^+)$ ($k_h(u, u_j^-)$) at u_j^+ (u_j^-) as δ_k, we can write:

$$(k_a - k_b)e^{-2\alpha u_0} = \delta_k, \tag{68}$$

from which we get:

$$u_0 = -\frac{1}{2\alpha} ln\left(\frac{\delta_k}{k_a - k_b}\right), \tag{69}$$

an expression providing positive values of u_0 for $\delta_k > 0$ since, by assumption, $k_a > k_b$ and $\alpha > 0$.

For practical purpose, δ_k is set equal to 10^{-20}, as suggested by the results of an extensive series of numerical tests; in such a way, we not only allow c^+ (c^-) to have a generalized tangent stiffness at u_j^+ (u_j^-) very close to the one of c_u (c_l), but we also avoid to make u_0 undefined, as it would happen if we set δ_k equal to zero in Eq. (69).

Finally, the parameter γ characterizes the shaping function $\psi(u)$, a positive convex function on $(-\infty, \infty)$ when $\gamma \neq 0$.

Note that assuming $\beta_1 = \beta_2 = \beta$ and $\gamma = 0$, we obtain the generalized tangent stiffness functions adopted in the Exponential Model described in Ref. [33].

4.2.2. Generalized force

We now derive the expressions of the upper (lower) limiting curve c_u (c_l) and of the generic loading (unloading) curve c^+ (c^-) required for the evaluation of the generalized force f during the generic loading (unloading) phase.

Upper (Lower) Limiting Curve

According to the definition (7) and to the assumption (63), we have:

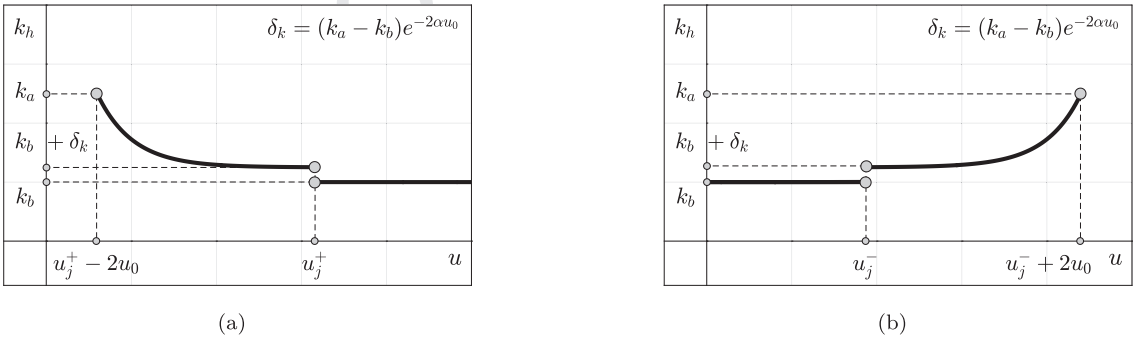

Fig. 9. Graph of the function k_h for the generic loading (a) and unloading (b) case (Asymmetric Exponential Model).

Please cite this article as: N. Vaiana, S. Sessa and L. Rosati, A generalized class of uniaxial rate-independent models for simulating asymmetric mechanical hysteresis phenomena, Mechanical Systems and Signal Processing, https://doi.org/10.1016/j.ymssp.2020.106984

$$f_e(u) = -(\beta_1+\beta_2)u + e^{\beta_1 u} - e^{-\beta_2 u}. \tag{70}$$

Hence, taking into account (66), (67), and (70), Eq. (11) becomes:

$$c_u(u) = -(\beta_1+\beta_2)u + e^{\beta_1 u} - e^{-\beta_2 u} + e^{\gamma u}\left(k_b u + f_0^+\right), \tag{71}$$

whereas Eq. (17) yields:

$$c_l(u) = -(\beta_1+\beta_2)u + e^{\beta_1 u} - e^{-\beta_2 u} + e^{\gamma u}\left(k_b u - f_0^-\right). \tag{72}$$

Generic Loading (Unloading) Curve

Because of the assumptions (64a) and (67), Eq. (21) specializes to:

$$f_h(u, u_j^+) = k_b u - \frac{(k_a - k_b)}{\alpha} e^{-\alpha\left(u - u_j^+ + 2u_0\right)}, \tag{73}$$

so that, recalling (66), (67), and (70), Eq. (25) yields:

$$c^+(u, u_j^+) = -(\beta_1+\beta_2)u + e^{\beta_1 u} - e^{-\beta_2 u} + e^{\gamma u}\left\{k_b u - \frac{(k_a - k_b)}{\alpha}\left[e^{-\alpha\left(u - u_j^+ + 2u_0\right)} - e^{-2\alpha u_0}\right] + f_0^+\right\}. \tag{74}$$

Similarly, on account of the assumptions (65a) and (67), Eq. (29) becomes:

$$f_h(u, u_j^-) = k_b u + \frac{(k_a - k_b)}{\alpha} e^{-\alpha\left(-u + u_j^- + 2u_0\right)}. \tag{75}$$

Hence, taking into account (66), (67), and (70), Eq. (33) yields:

$$c^-(u, u_j^-) = -(\beta_1+\beta_2)u + e^{\beta_1 u} - e^{-\beta_2 u} + e^{\gamma u}\left\{k_b u + \frac{(k_a - k_b)}{\alpha}\left[e^{-\alpha\left(-u + u_j^- + 2u_0\right)} - e^{-2\alpha u_0}\right] - f_0^-\right\}. \tag{76}$$

4.2.3. History variable

Invoking (70) and (73), and taking into account the assumptions (66) and (67), Eq. (35) specializes to:

$$-(\beta_1+\beta_2)u_P + e^{\beta_1 u_P} - e^{-\beta_2 u_P} + e^{\gamma u_P}\left[k_b u_P - \frac{(k_a - k_b)}{\alpha} e^{-\alpha\left(u_P - u_j^+ + 2u_0\right)} + k_b u_j^+ + f_0^+ - k_b u_j^+ + \frac{(k_a - k_b)}{\alpha} e^{-2\alpha u_0}\right] = f_P,$$

from which we obtain the expression of the history variable for the generic loading case:

$$u_j^+ = u_P + 2u_0 + \frac{1}{\alpha} ln\left\{\frac{\alpha}{(k_a - k_b)}\left[e^{-\gamma u_P}\left(-(\beta_1+\beta_2)u_P + e^{\beta_1 u_P} - e^{-\beta_2 u_P}\right) + k_b u_P + \frac{(k_a - k_b)}{\alpha} e^{-2\alpha u_0} + f_0^+ - e^{-\gamma u_P} f_P\right]\right\}. \tag{78}$$

Similarly, using (70) and (75), and taking into account (66) and (67), Eq. (37) becomes:

$$-(\beta_1+\beta_2)u_P + e^{\beta_1 u_P} - e^{-\beta_2 u_P} + e^{\gamma u_P}\left[k_b u_P + \frac{(k_a - k_b)}{\alpha} e^{-\alpha\left(-u_P + u_j^- + 2u_0\right)} + k_b u_j^- - f_0^- - k_b u_j^- - \frac{(k_a - k_b)}{\alpha} e^{-2\alpha u_0}\right] = f_P,$$

from which we obtain the expression of the history variable for the generic unloading case:

$$u_j^- = u_P - 2u_0 - \frac{1}{\alpha} ln\left\{-\frac{\alpha}{(k_a - k_b)}\left[e^{-\gamma u_P}\left(-(\beta_1+\beta_2)u_P + e^{\beta_1 u_P} - e^{-\beta_2 u_P}\right) + k_b u_P - \frac{(k_a - k_b)}{\alpha} e^{-2\alpha u_0} - f_0^- - e^{-\gamma u_P} f_P\right]\right\}. \tag{80}$$

Note that Eq. (78) (Eq. (80)) may provide positive or negative values of u_j^+ (u_j^-) according to the coordinates of the initial point $P:(u_P, f_P)$ of c^+ (c^-). In any case, the argument of the logarithm in Eqs. (78) and (80) is always positive if $k_a > k_b, k_a > 0, \alpha > 0$, and $u_0 > 0$. Actually, looking at Fig. 6, we observe that the generalized displacement u_j^+ (u_j^-) can have two extreme values, namely $u_P + 2u_0$ ($u_P - 2u_0$) when P belongs to the lower (upper) limiting curve, and u_P when P lies on the upper (lower) limiting curve; thus, the argument of the logarithm in Eq. (78) (Eq. (80)) has to be equal to 1 in the former case, and equal to $\delta_k (k_a - k_b)^{-1}$ in the latter. Being $\delta_k \ll (k_a - k_b), \delta_k (k_a - k_b)^{-1}$ represents the minimum value of the logarithm argument, a quantity that is always positive since $\delta_k > 0$ and $k_a > k_b$.

4.2.4. Expression of f_0^+ (f_0^-)

We determine the expression of f_0^+ (f_0^-), referred to as *internal model parameter* since it can be expressed as a function of the model parameters described in 4.2.1. In particular, after imposing that $f_0^+ = f_0^- = f_0$, we use Eqs. (40), (67), and (73) to get:

Please cite this article as: N. Vaiana, S. Sessa and L. Rosati, A generalized class of uniaxial rate-independent models for simulating asymmetric mechanical hysteresis phenomena, Mechanical Systems and Signal Processing, https://doi.org/10.1016/j.ymssp.2020.106984

$$k_b\left(u_j^+ - 2u_0\right) - \frac{(k_a - k_b)}{\alpha} + 2k_b u_0 + 2f_0 - k_b u_j^+ + \frac{(k_a - k_b)}{\alpha} e^{-2\alpha u_0} = 0, \tag{81}$$

from which we obtain:

$$f_0 = \frac{(k_a - k_b)}{2\alpha}\left(1 - e^{-2\alpha u_0}\right). \tag{82}$$

Note that Eq. (82) provides a positive value of f_0, being $k_a > k_b, \alpha > 0$, and $u_0 > 0$.

It can be easily shown that the same expression of f_0 can be derived adopting Eq. (43) instead of Eq. (40).

4.2.5. Hysteresis loop shapes

As shown in Table 2, the Asymmetric Exponential Model is able to simulate six different types of the generalized force-displacement hysteresis loop shape according to the values of the parameters β_1 and β_2; specifically, when $\gamma = 0$, it can reproduce two symmetric hysteresis loop shape types, namely SS1 and SS2, and four asymmetric hysteresis loop shape types, namely AS1, AS2, AS3, and AS4. The hysteresis loop shapes obtained for $\gamma \neq 0$ will be presented later.

Fig. 10 illustrates six hysteresis loops having shape type SS1, SS2, AS1, AS2, AS3, and AS4, respectively, simulated by imposing a generalized sinusoidal displacement with unit amplitude and frequency and by using the six model parameters listed in Table 3. In particular, Fig. 10a (10b) presents a symmetric hysteresis loop bounded by two parallel straight lines (curves), whereas Fig. 10c and e (10d and 10f) show an asymmetric hysteresis loop limited by two non-parallel curves having no (one) inflection point. Such hysteresis loops are typical of several hysteretic mechanical systems and materials [2–4,8,11,13,18,21,32,36], as described in Section 2.

Fig. 11 shows the variation of the size and/or shape of the hysteresis loops, simulated by applying a generalized sinusoidal displacement with unit amplitude and frequency, due to each model parameters, namely k_a, k_b, α, β_1, and β_2, when $\gamma = 0$. More specifically, looking at the hysteresis loops of Fig. 11a, obtained for $k_b = 0.5$, $\alpha = 5$, $\beta_1 = 0$, $\beta_2 = 0$, and three different values of k_a, that is, 5, 10, and 15, we can not only observe that the larger (smaller) is k_a, the larger (smaller) is the hysteresis loop size, but also that such a parameter does not affect the hysteresis loop shape.

Fig. 11b presents hysteresis loops reproduced by using $k_a = 5$, $\alpha = 5$, $\beta_1 = 0$, $\beta_2 = 0$, and three values of k_b, that is, 0, 0.5, and 1. We can note that increasing (decreasing) k_b, the hysteresis loop rotates counterclockwise (clockwise) and its size slightly decreases (increases).

Looking at the hysteresis loops of Fig. 11c, obtained for $k_a = 5, k_b = 0.5, \beta_1 = 0, \beta_2 = 0$, and three different values of α, that is, 5, 10, and 15, we can not only notice that the larger (smaller) is α, the smaller (larger) is the hysteresis loop size, but also that such a parameter does not affect the hysteresis loop shape.

Fig. 11d shows hysteresis loops reproduced by adopting $k_a = 5$, $k_b = 0.5$, $\alpha = 5$, and three values of $\beta_1 = \beta_2 = \beta$, that is, 0, 1, and 1.5. We can observe that such a parameter modifies the hysteresis loop shape in such a way that it remains symmetric.

Finally, looking at the hysteresis loops of Fig. 11e (11f), obtained for $k_a = 5$, $k_b = 0.5$, $\alpha = 5$, $\beta_2 = 0$ ($k_a = 5$, $k_b = 0.5$, $\alpha = 5$, $\beta_1 = 0$), and three different values of β_1 (β_2), that is, 0, 1, and 1.5, we can note that such a parameter modifies the hysteresis loop shape in such a way that it becomes asymmetric.

The six different types of hysteresis loop shape, summarized in Table 2 and obtained for $\gamma = 0$, can be conveniently modified by selecting a different value of γ, that is, $\gamma \neq 0$. In particular, Fig. 12 shows how each hysteresis loop of Fig. 10 (black line) is modified by selecting a positive value of γ listed in Table 4. Looking carefully at the modified hysteresis loops (red line), we can observe that, when it is positive, such a parameter allows one to increase (decrease) the generalized tangent stiffness as well as the vertical distance between the two limiting curves for $u > 0$ ($u < 0$).

On the contrary, when it is negative, such a parameter allows one to decrease (increase) the generalized tangent stiffness as well as the vertical distance between the two limiting curves for $u > 0$ ($u < 0$). The figure showing the influence of a negative value of γ on the shape of the hysteresis loops of Fig. 10 is omitted for brevity.

Such a modeling aspect is of fundamental importance in the simulation of the asymmetric hysteresis phenomena displayed by some rate-independent mechanical systems and materials [3,4,8,32].

Table 2
Hysteresis loop shape types that can be simulated by the Asymmetric Exponential Model for $\gamma = 0$.

Shape type	Obtained for
SS1	$\beta_1 = \beta_2 = \beta = 0$
SS2	$\beta_1 = \beta_2 = \beta > 0$
AS1	$\beta_1 > \beta_2 = 0$
AS2	$\beta_1 > \beta_2 > 0$
AS3	$\beta_2 > \beta_1 = 0$
AS4	$\beta_2 > \beta_1 > 0$

Please cite this article as: N. Vaiana, S. Sessa and L. Rosati, A generalized class of uniaxial rate-independent models for simulating asymmetric mechanical hysteresis phenomena, Mechanical Systems and Signal Processing, https://doi.org/10.1016/j.ymssp.2020.106984

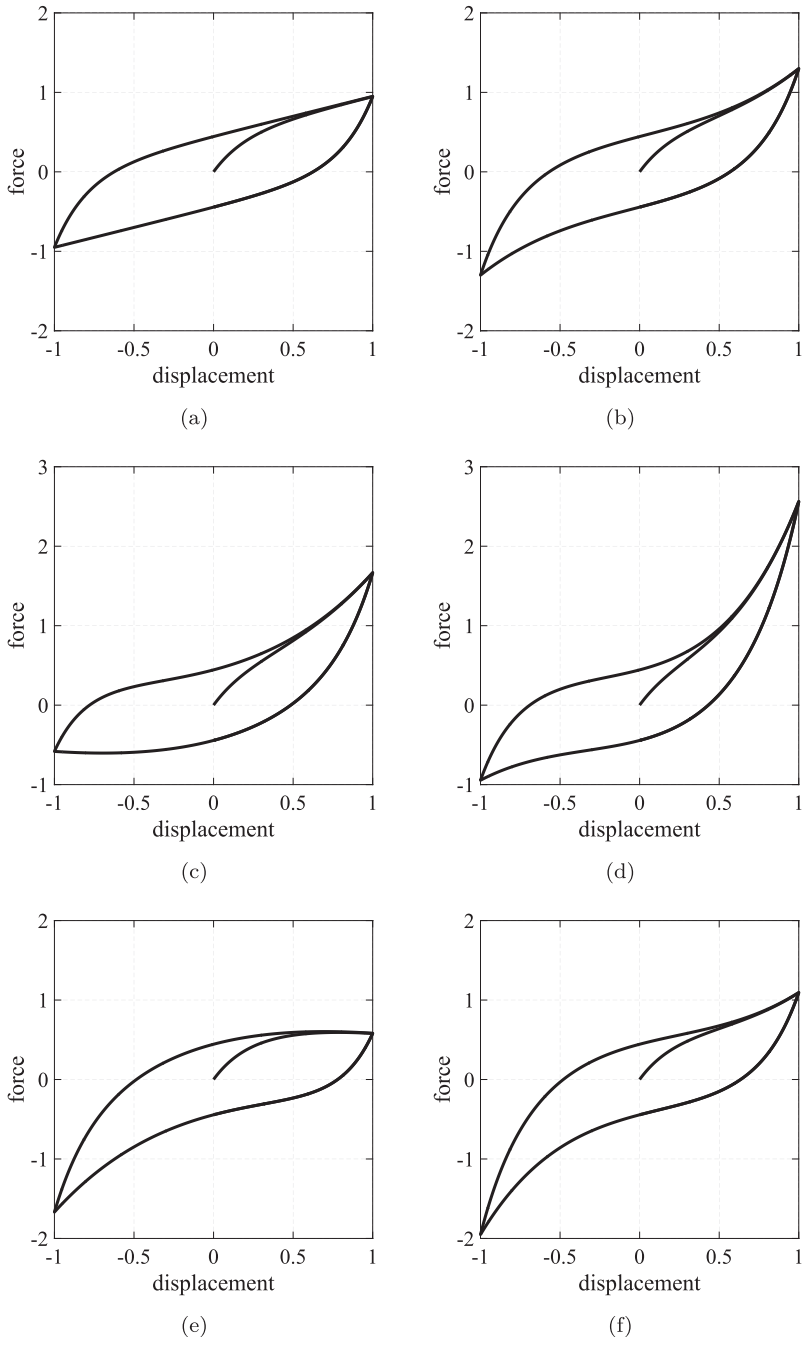

Fig. 10. Hysteresis loops simulated by using the Asymmetric Exponential Model parameters given in Table 3.

Table 3
Asymmetric Exponential Model parameters adopted for the hysteresis loops in Fig. 10.

	k_a	k_b	α	β_1	β_2	γ
(a)	5.0	0.5	5.0	0.0	0.0	0.0
(b)	5.0	0.5	5.0	1.0	1.0	0.0
(c)	5.0	0.5	5.0	1.0	0.0	0.0
(d)	5.0	0.5	5.0	1.5	1.0	0.0
(e)	5.0	0.5	5.0	0.0	1.0	0.0
(f)	5.0	0.5	5.0	1.0	1.3	0.0

Please cite this article as: N. Vaiana, S. Sessa and L. Rosati, A generalized class of uniaxial rate-independent models for simulating asymmetric mechanical hysteresis phenomena, Mechanical Systems and Signal Processing, https://doi.org/10.1016/j.ymssp.2020.106984

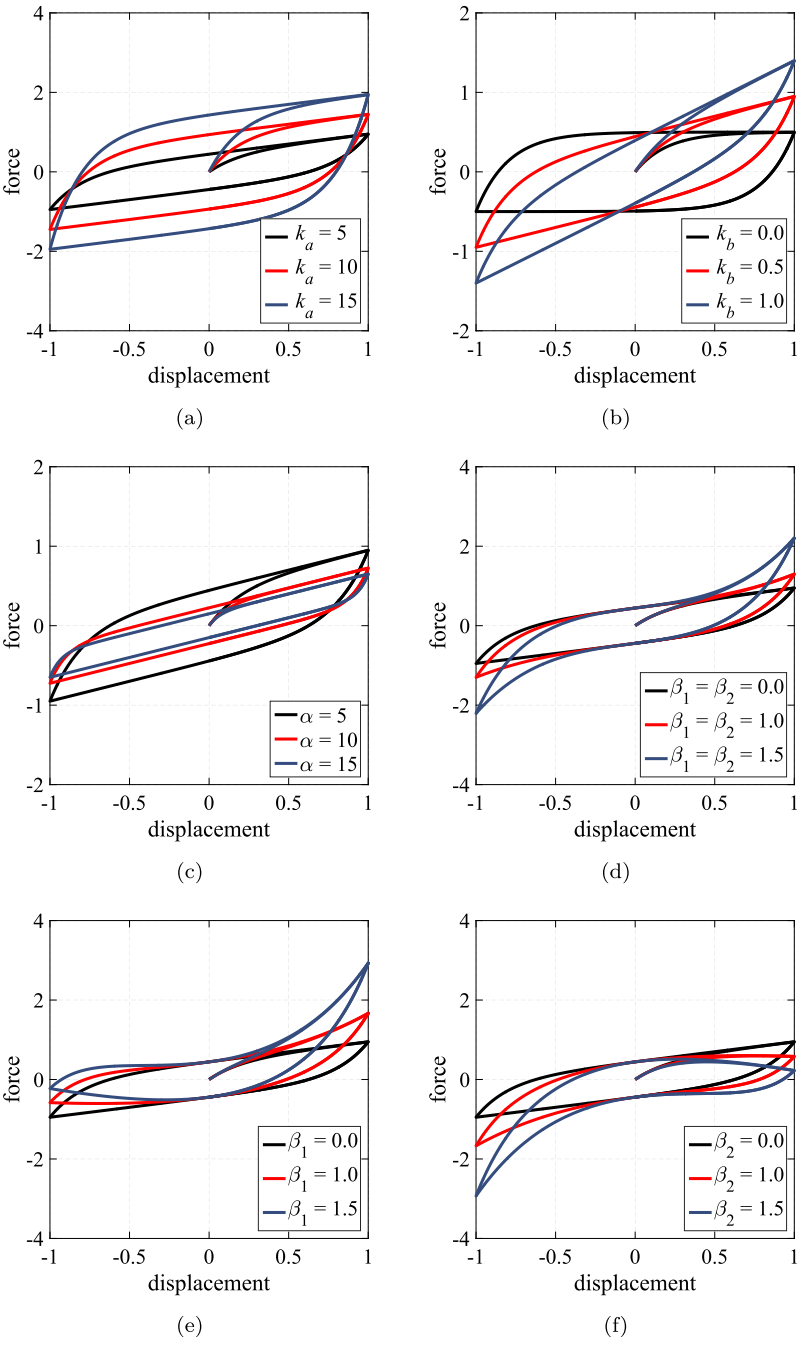

Fig. 11. Influence of the Asymmetric Exponential Model parameters on the size and/or shape of the hysteresis loops.

4.3. Computer implementation

We now illustrate the schematic flowcharts of the Asymmetric Bilinear and Exponential Models to help the reader with the computer implementation. To this end, we suppose to apply a time-dependent force to a rate-independent mechanical system or material and to adopt a displacement-driven solution scheme to evaluate its nonlinear response. Hence, under these assumptions, over a generic time step Δt, we know the generalized displacements $u_{t-\Delta t}$ and u_t, the generalized velocities $\dot{u}_{t-\Delta t}$ and $\dot{u}_t$, as well as the generalized force $f_{t-\Delta t}$, and we need to evaluate f_t.

The implementation scheme of the Asymmetric Bilinear (Exponential) Model is summarized in Table 5a (5b). Such an algorithm consists of two parts. In the first one, denominated *Initial settings*, we (first) assign the model parameters (and then

Please cite this article as: N. Vaiana, S. Sessa and L. Rosati, A generalized class of uniaxial rate-independent models for simulating asymmetric mechanical hysteresis phenomena, Mechanical Systems and Signal Processing, https://doi.org/10.1016/j.ymssp.2020.106984

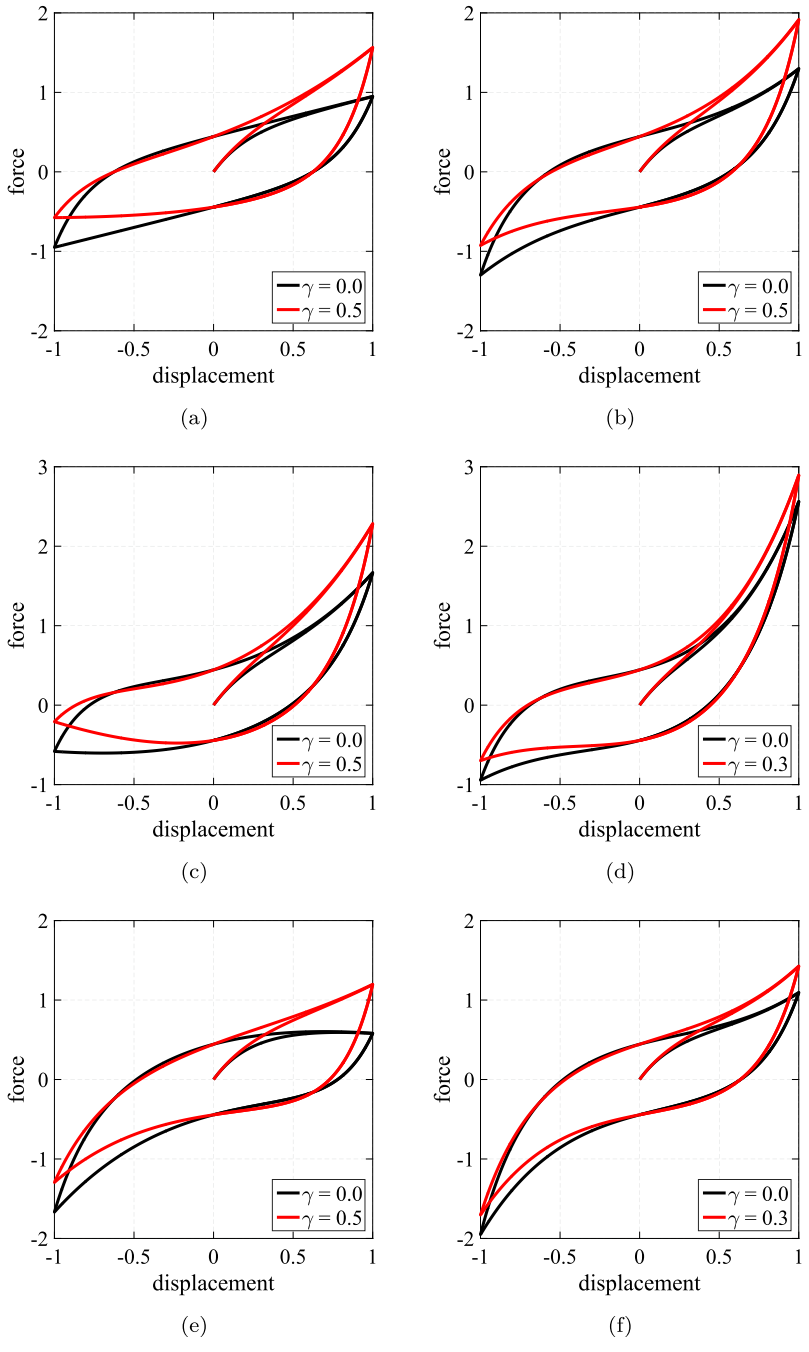

Fig. 12. Hysteresis loops simulated by using the Asymmetric Exponential Model parameters given in Table 3 (black line) and in Table 4 (red line). (For interpretation of the references to color in this figure legend, the reader is referred to the web version of this article.)

Table 4
Asymmetric Exponential Model parameters adopted for the hysteresis loops in Fig. 12.

	k_a	k_b	α	β_1	β_2	γ
(a)	5.0	0.5	5.0	0.0	0.0	0.5
(b)	5.0	0.5	5.0	1.0	1.0	0.5
(c)	5.0	0.5	5.0	1.0	0.0	0.5
(d)	5.0	0.5	5.0	1.5	1.0	0.3
(e)	5.0	0.5	5.0	0.0	1.0	0.5
(f)	5.0	0.5	5.0	1.0	1.3	0.3

Please cite this article as: N. Vaiana, S. Sessa and L. Rosati, A generalized class of uniaxial rate-independent models for simulating asymmetric mechanical hysteresis phenomena, Mechanical Systems and Signal Processing, https://doi.org/10.1016/j.ymssp.2020.106984

Table 5
Asymmetric Bilinear Model Algorithm.

1. Initial settings.	
1.1	Set the six model parameters: k_a^+, k_b^+, f_0^+, k_a^-, k_b^-, and f_0^-.
2. Calculations at each time step.	
2.1	If $t = \Delta t$ or $s_t s_{t-\Delta t} < 0$, update the model parameters: $k_a = k_a^+$ (k_a^-), $k_b = k_b^+$ (k_b^-), and $f_0 = f_0^+$ (f_0^-) if $s_t > 0$ $(s_t < 0)$, the history variable [see (56) and (58)]: $u_j = \frac{k_a u_{t-\Delta t} + f_0 s_t - f_{t-\Delta t}}{k_a - k_b}$, and the internal model parameter [see (60) and (62)]: $u_0 = \frac{(k_b^+ - k_b^-)u_j + f_0^+ + f_0^-}{2(k_a^+ - k_b^-)} \left(\frac{(k_b^+ - k_b^-)u_j + f_0^+ + f_0^-}{2(k_a^- - k_b^+)} \right)$ if $s_t > 0$ $(s_t < 0)$.
2.2	Evaluate the generalized force at time t: if $u_j s_t - 2u_0 < u_t s_t < u_j s_t$: $f_t = k_a(u_t - u_j) + k_b u_j + f_0 s_t$; [see (52) and (54)], otherwise: $f_t = k_b u_t + f_0 s_t$; [see (49) and (50)].

Table 5b. Asymmetric Exponential Model Algorithm

1. Initial settings.	
1.1	Set the six model parameters: k_a, k_b, α, β_1, β_2, and γ.
1.2	Compute the internal model parameters [see (69) and (82)]: $u_0 = -\frac{1}{2\alpha} ln\left(\frac{\delta_k}{k_a - k_b}\right)$ and $f_0 = \frac{k_a - k_b}{2\alpha}(1 - e^{-2\alpha u_0})$, with $\delta_k = 10^{-20}$.
2. Calculations at each time step.	
2.1	If $t = \Delta t$ or $s_t s_{t-\Delta t} < 0$, update the history variable [see (78) and (80)]: $u_j = u_{t-\Delta t} + 2u_0 s_t + \frac{s_t}{\alpha} ln\left[\frac{\alpha s_t}{k_a - k_b}\left(e^{-\gamma u_{t-\Delta t}}(f_e)_{t-\Delta t} + k_b u_{t-\Delta t} + \frac{k_a - k_b}{\alpha} s_t e^{-2\alpha u_0} + f_0 s_t - e^{-\gamma u_{t-\Delta t}} f_{t-\Delta t}\right)\right]$, with $(f_e)_{t-\Delta t} = -(\beta_1 + \beta_2)u_{t-\Delta t} + e^{\beta_1 u_{t-\Delta t}} - e^{-\beta_2 u_{t-\Delta t}}$.
2.2	Evaluate the generalized force at time t: if $u_j s_t - 2u_0 < u_t s_t < u_j s_t$: $f_t = (f_e)_t + e^{\gamma u_t}\left\{k_b u_t - s_t \frac{k_a - k_b}{\alpha}\left[e^{-\alpha(u_t s_t - u_j s_t + 2u_0)} - e^{-2\alpha u_0}\right] + f_0 s_t\right\}$; [see (74) and (76)], otherwise: $f_t = (f_e)_t + e^{\gamma u_t}(k_b u_t + f_0 s_t)$; [see (71) and (72)], with $(f_e)_t = -(\beta_1 + \beta_2)u_t + e^{\beta_1 u_t} - e^{-\beta_2 u_t}$.

we evaluate the internal ones). In the second part, denominated *Calculations at each time step*, we update the model parameters, the history variable, and the internal model parameter (we update the history variable) if we are at the first time step, that is, $t = \Delta t$, or if the sign of $\dot{u}_t$, namely $s_t = sgn(\dot{u}_t)$, changes with respect to the one of $\dot{u}_{t-\Delta t}$, namely $s_{t-\Delta t} = sgn(\dot{u}_{t-\Delta t})$; finally, we compute the generalized force f_t.

5. Verification of the Asymmetric Exponential Model

In this section we present the validation of the Asymmetric Exponential Model (AEM). Specifically, we first carry out the experimental verification by simulating some experimental asymmetric hysteresis loops selected from the literature and, to better illustrate the features of the developed model, we reproduce the same experimental results by employing the Generalized Bouc-Wen Model (GBWM) formulated by Song and Der Kiureghian [31]. Then, we prove the numerical accuracy and the computational efficiency of the proposed model by performing some nonlinear time history analyses on a rate-independent hysteretic mechanical system and comparing the results with those computed by adopting the Modified Bouc-Wen Model (MBWM) formulated by Ni et al. [23].

5.1. Experimental verification

In order to show the capability of the developed model to simulate complex asymmetric hysteresis phenomena typical of several mechanical systems and materials subjected to a generalized cyclic displacement history with different amplitudes, we compare the results analytically predicted with the experimental ones. In particular, to perform such an experimental verification, we adopt the experimental hysteresis loops obtained during the quasi-static tests conducted on two different types of spring connectors by Filiatrault and Kremmidas [13].

5.1.1. Description of tested spring connectors

The two tested flexible connectors, namely Spring Type A and Spring Type B, typically used in electrical substations to allow electrical rigid bus conductors to accommodate thermal effects, consist of three parallel straps, each one constituted

by a pair of copper alloy bars. The former is an asymmetric device having one transverse and one axial terminal pad, whereas the latter is a symmetric device having two transverse terminal pads.

These devices show a highly asymmetric hysteretic behavior due to geometric and material nonlinearities, as well as to contact and friction between the copper alloy bars; such a behavior is also characterized by an increase of the transverse tangent stiffness with increasing positive transverse displacements due to the so-called *tension stiffening effect*. Additional details regarding the above-described devices and the experimental tests setup can be found in Ref. [13].

5.1.2. Simulation of experimental asymmetric hysteresis loops

In Fig. 13a (13b), we compare the analytical and experimental results obtained by slowly imposing, to the above-described Spring Type A (Spring Type B), a transverse displacement history characterized by a sequence of six sets of cycles having an increasing amplitude.

We can observe that the agreement between the experimental asymmetric restoring force-displacement hysteresis loops and the analytical ones, simulated by employing the Asymmetric Exponential Model, is satisfactory in both cases. The adopted six model parameters, evaluated by fitting the experimental data by means of an improved version of the inverse identification strategy recently proposed by Sessa et al. [29], are listed in Table 6. The properties of such an adopted identification procedure will be explained in details in a future paper.

In addition, we note that the proposed model is not only able to simulate the highly asymmetric shape of the experimental hysteresis loops but it is also capable of well simulating the increase of the transverse tangent stiffness occurring in such devices, for positive values of the transverse displacement, due to the tension stiffening effect.

5.1.3. Comparisons with the generalized Bouc-Wen model

To better illustrate the features of the developed model, the same experimental asymmetric hysteresis loops are simulated by means of the Generalized Bouc-Wen Model formulated by Ref. [31]. This differential model, representing a modified version of the Bouc-Wen model [7,39,40], has been specifically proposed to reproduce highly asymmetric hysteresis phenomena. In particular, it allows us to evaluate the restoring force of the above-described spring connectors as follows:

$$f(u) = aku + (1-a)kz, \tag{83}$$

where a represents a dimensionless parameter, k is a parameter having dimension of stiffness, whereas z is a variable having dimension of displacement; the latter is computed by solving the following first-order nonlinear ordinary differential equation:

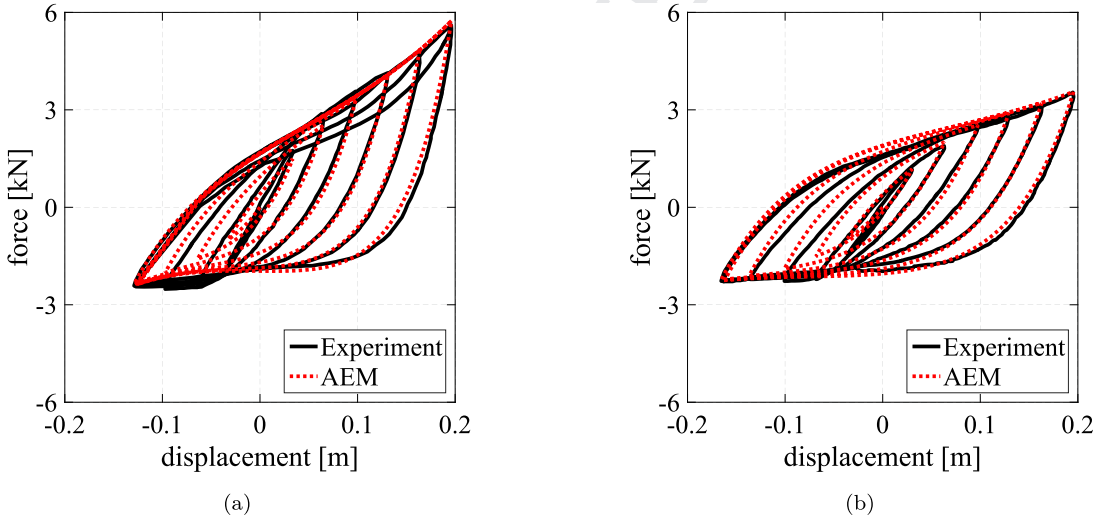

Fig. 13. Comparisons of experimental and analytical asymmetric hysteresis loops, simulated by using the AEM parameters given in Table 6: Spring Type A (a) and Spring Type B (b).

Table 6
AEM parameters used for simulating hysteresis loops in Fig. 13.

	k_a [kN m^{-1}]	k_b [kN m^{-1}]	α [m^{-1}]	β_1 [kN m^{-1}]	β_2 [kN m^{-1}]	γ [m^{-1}]
(a)	80.0	5.0	18.0	2.0	8.0	3.8
(b)	70.0	1.5	15.0	5.0	5.0	1.2

Please cite this article as: N. Vaiana, S. Sessa and L. Rosati, A generalized class of uniaxial rate-independent models for simulating asymmetric mechanical hysteresis phenomena, Mechanical Systems and Signal Processing, https://doi.org/10.1016/j.ymssp.2020.106984

$$\dot{z} = \dot{u}\{A - [b_1 sign(\dot{u}z) + b_2 sign(u\dot{u}) + b_3 sign(uz) + b_4 sign(\dot{u}) + b_5 sign(z) + b_6 sign(u)]|z|^n\}, \tag{84}$$

where A, b_1, b_2, b_3, b_4, b_5, b_6, and n are parameters defining the shape of the hysteresis loop.

In Fig. 14a (14b), we compare the experimental hysteresis loops of Spring Type A (Spring Type B) with those predicted by means of the Generalized Bouc-Wen Model; the adopted ten model parameters, that have been calibrated by Ref. [31], are listed in Table 7 for the reader's convenience.

Comparing Figs. 13 and 14, we can observe that the Asymmetric Exponential Model is more accurate than the Generalized Bouc-Wen Model; indeed, the former is not only able of simulating smooth hysteresis loops, that is, hysteresis loops having a left-hand tangent stiffness at $u = 0$ equal to the right-hand one, but it is also able to better simulate the increase of the tangent stiffness due to the tension stiffening effect. Furthermore, looking at Tables 6 and 7, we can also note that the proposed model needs a smaller number of parameters that have a clear graphical meaning, as shown in 4.2.5.

5.2. Numerical verification and computational efficiency

In this subsection we simulate the nonlinear dynamic response of a single degree of freedom mechanical system, having a rate-independent asymmetric hysteretic behavior, by modeling the generalized force using the Asymmetric Exponential Model illustrated in Section 4. We perform the analyses for two different generalized external forces, namely a harmonic force and a random force.

In order to show the numerical accuracy and the computational efficiency of the proposed model, we compare the analyses results and the related computational times with those obtained by employing a modified version of the Bouc-Wen model, formulated by Ni et al. [23], to reproduce the generalized force of the analyzed mechanical system.

5.3. Analyzed mechanical system with asymmetric hysteretic behavior

Let us introduce the nonlinear equilibrium equation of the analyzed Single-Degree-Of-Freedom (SDOF) mechanical system having a rate-independent asymmetric hysteretic behavior. To this end, we denote by u and $\ddot{u}$ the generalized displacement and acceleration, respectively, and by $p(t)$ the generalized external force depending on time t. Hence, invoking the d'Alembert's principle, we get:

$$m\ddot{u} + f(u) = p(t), \tag{85}$$

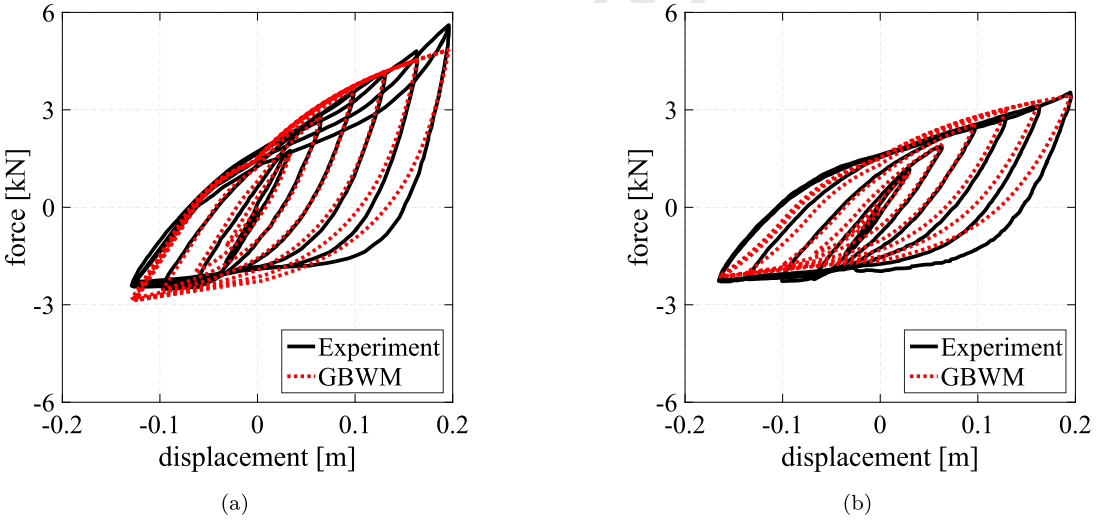

Fig. 14. Comparisons of experimental and analytical asymmetric hysteresis loops, simulated by using the GBWM parameters given in Table 7: Spring Type A (a) and Spring Type B (b).

Table 7
GBWM parameters used for simulating hysteresis loops in Fig. 14.

	a	k [kN m^{-1}]	A	b_1	b_2	b_3	b_4	b_5	b_6	n
(a)	0.1	49.2	1.0	0.4700	−0.1180	0.0294	0.1150	−0.1210	−0.1120	1.0
(b)	0.1	35.6	1.0	0.4190	−0.1930	0.1740	0.0901	−0.1560	−0.0564	1.0

Please cite this article as: N. Vaiana, S. Sessa and L. Rosati, A generalized class of uniaxial rate-independent models for simulating asymmetric mechanical hysteresis phenomena, Mechanical Systems and Signal Processing, https://doi.org/10.1016/j.ymssp.2020.106984

where m is the mass of the system and $f(u)$ represents its generalized force. In particular, $m = 1$ Ns^2 m^{-1}, whereas the generalized force-displacement hysteresis loop (Fig. 15a), described by $f(u)$ when such a system is subjected to a generalized sinusoidal displacement with amplitude of 0.25 m and unit frequency (Fig. 15b), is bounded by two non-parallel limiting curves having no inflection point.

5.4. Applied generalized external forces

In Fig. 16, we show the two different types of applied generalized external forces adopted to perform the nonlinear time history analyses, namely the harmonic force and the random force. In particular, the former, illustrated in Fig. 16a, is a sinu-

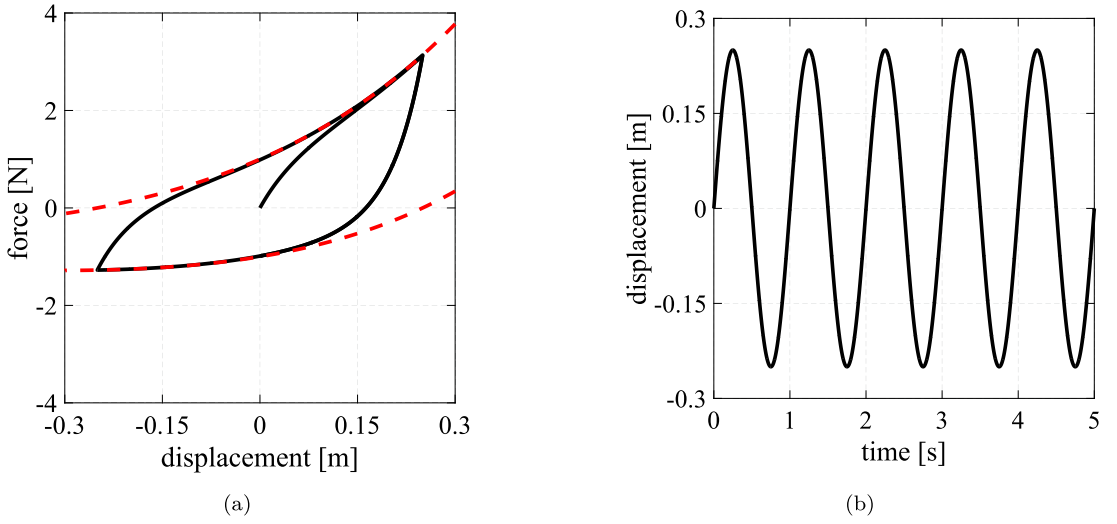

Fig. 15. Generalized force-displacement asymmetric hysteresis loop (a) obtained by applying a generalized harmonic displacement (b) to the mechanical system described by Eq. (85).

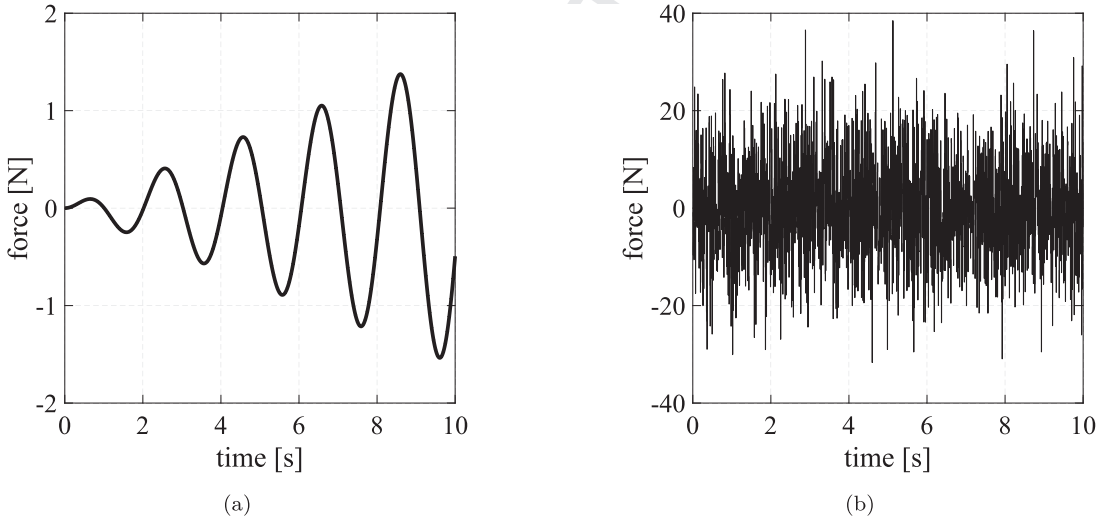

Fig. 16. Applied generalized external harmonic (a) and random (b) force.

Table 8
AEM parameters adopted in the nonlinear time history analyses.

k_a [N m^{-1}]	k_b [N m^{-1}]	α [m^{-1}]	β_1 [N m^{-1}]	β_2 [N m^{-1}]	γ [m^{-1}]
44.0	4.0	20.0	0.0	0.0	1.8

Please cite this article as: N. Vaiana, S. Sessa and L. Rosati, A generalized class of uniaxial rate-independent models for simulating asymmetric mechanical hysteresis phenomena, Mechanical Systems and Signal Processing, https://doi.org/10.1016/j.ymssp.2020.106984

Table 9
MBWM parameters adopted in the nonlinear time history analyses.

a_1	a_2 [m^{-1}]	k_1 [N m^{-1}]	k_2 [N m^{-2}]	k_3 [N m^{-3}]	A [N m^{-1}]	b_1	b_2	n
2.718	1.8	4.0	0.0	0.0	20.0	20.0	0.0	1.05

Table 10
NLTHAs results – Harmonic force.

	tct [s]	$tctp$	u[m]		$\dot{u}$ [ms^{-1}]		$\ddot{u}$ [ms^{-2}]	
			max	min	max	min	max	min
MBWM	8.942	–	0.2264	−0.2925	0.8038	−0.8275	2.0849	−3.6322
AEM	0.059	0.66%	0.2258	−0.2901	0.7997	−0.8244	2.0791	−3.6185

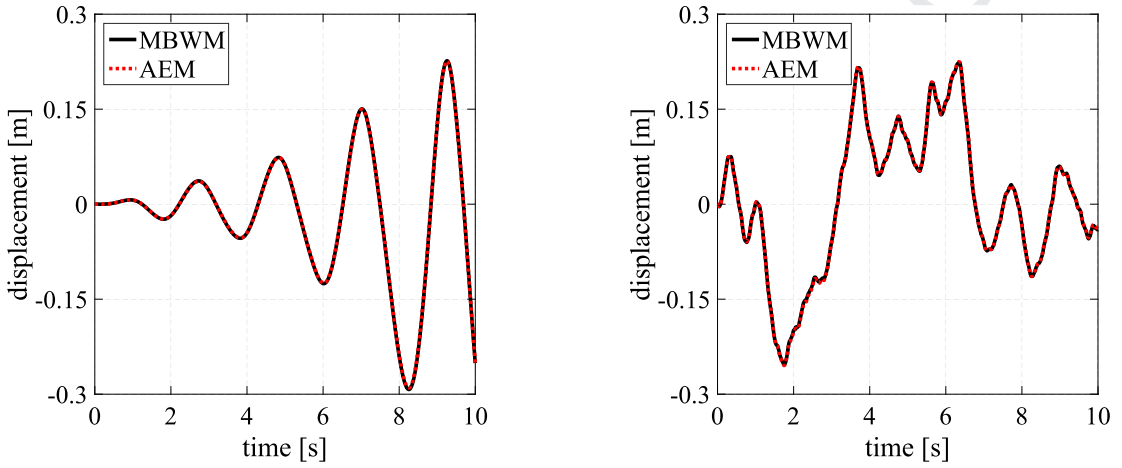

Fig. 17. Generalized displacement time history obtained for the harmonic (a) and random (b) force.

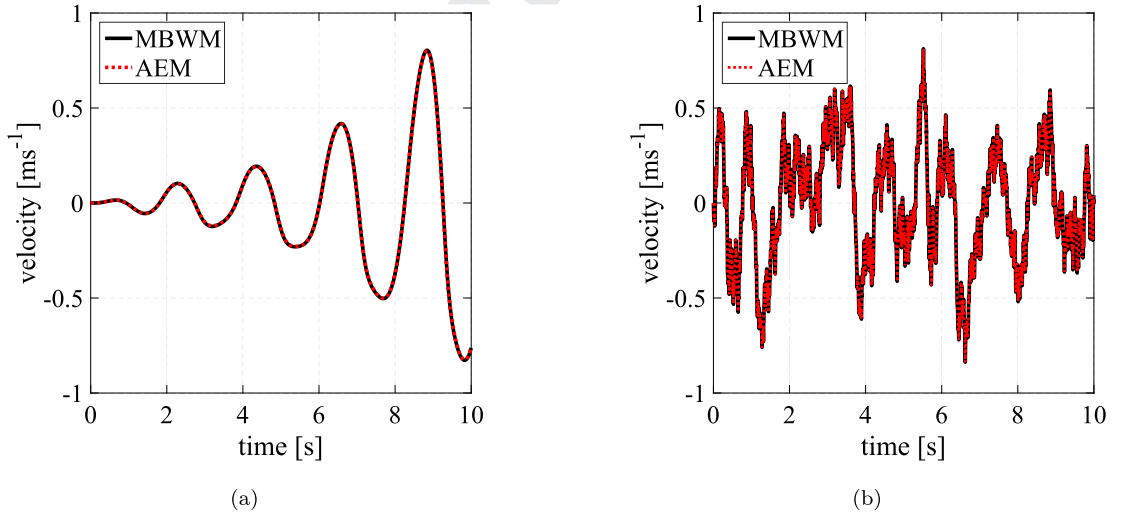

Fig. 18. Generalized velocity time history obtained for the harmonic (a) and random (b) force.

Please cite this article as: N. Vaiana, S. Sessa and L. Rosati, A generalized class of uniaxial rate-independent models for simulating asymmetric mechanical hysteresis phenomena, Mechanical Systems and Signal Processing, https://doi.org/10.1016/j.ymssp.2020.106984

soidal force characterized by an amplitude p_0, that increases linearly with time from 0 to 1.6 N, and a forcing frequency $\omega_p = 3.11$ rad/s. The latter, illustrated in Fig. 16b, is a Gaussian white noise characterized by an intensity $iwn = 10$ N. Both generalized external forces have a time duration $t_d = 10$ s.

5.5. Asymmetric models parameters

To illustrate the numerical features of the developed model, the results of the nonlinear time history analyses are compared with those obtained by employing the Modified Bouc-Wen Model formulated by Ni et al. [23]. This differential model, representing an improved version of the Bouc-Wen model [7,39,40], has been specifically proposed to reproduce highly asymmetric hysteresis phenomena. Together with the Generalized Bouc-Wen Model, described in 5.1.3, it represents one of the most widespread asymmetric hysteretic models available in the literature. In particular, it allows us to evaluate the generalized force of the above-described rate-independent mechanical system as follows:

$$f(u) = a_1^{(a_2 u)}\left(k_1 u + k_2 sign(u)u^2 + k_3 u^3 + z\right), \tag{86}$$

where z represents a variable, having dimension of generalized force, that is computed by solving the following first-order nonlinear ordinary differential equation:

$$\dot{z} = \dot{u}\left\{A - [b_1 sign(\dot{u}z) + b_2]|z|^n\right\}, \tag{87}$$

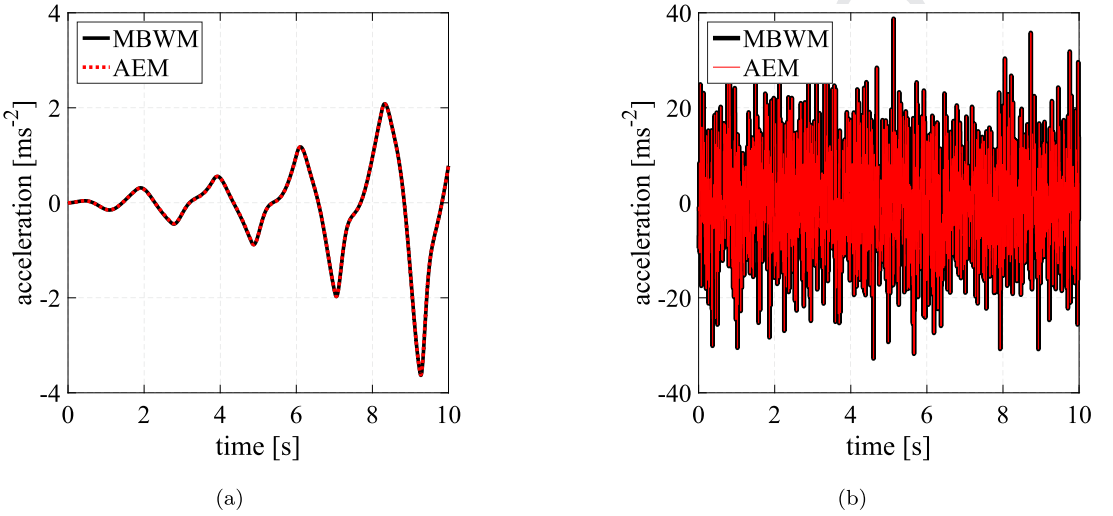

Fig. 19. Generalized acceleration time history obtained for the harmonic (a) and random (b) force.

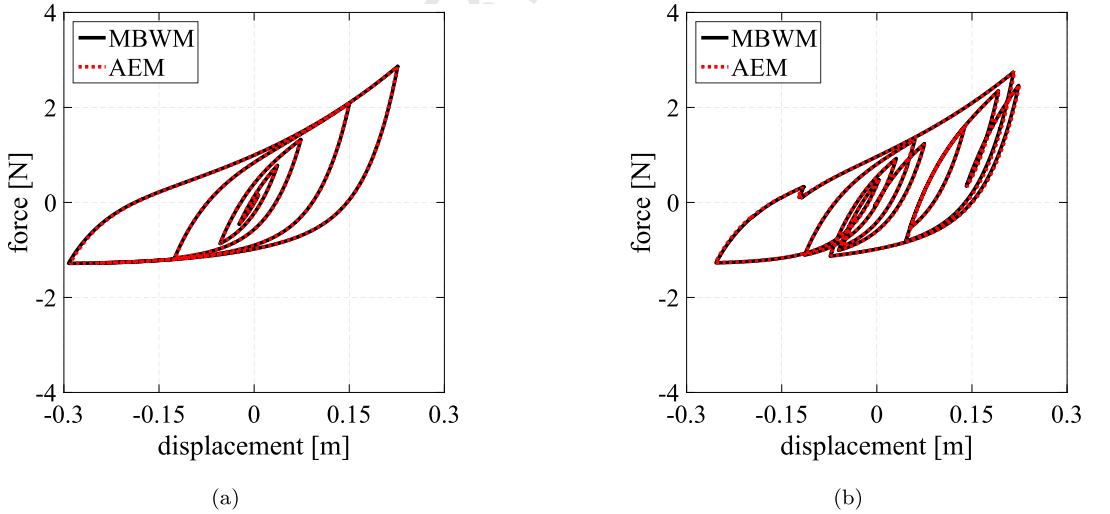

Fig. 20. Generalized force-displacement asymmetric hysteresis loops obtained for the harmonic (a) and random (b) force.

Please cite this article as: N. Vaiana, S. Sessa and L. Rosati, A generalized class of uniaxial rate-independent models for simulating asymmetric mechanical hysteresis phenomena, Mechanical Systems and Signal Processing, https://doi.org/10.1016/j.ymssp.2020.106984

Table 11
NLTHAs results – Random force.

	tct [s]	*tctp*	*u* m		$\dot{u}$ [ms^{-1}]		$\ddot{u}$ [ms^{-2}]	
			max	min	max	min	max	min
MBWM	9.023	–	0.2236	−0.2536	0.8121	−0.8377	38.7653	−32.7983
AEM	0.062	0.69%	0.2249	−0.2547	0.8109	−0.8380	38.7682	−32.7979

whereas a_1, a_2, k_1, k_2, k_3, A, b_1, b_2, and n are the nine model parameters.

To perform the analyses, we have calibrated the parameters of the Asymmetric Exponential Model (Modified Bouc-Wen Model) through an analytical fitting of the asymmetric hysteresis loop, illustrated in Fig. 15a, that characterizes the behavior of the analyzed mechanical system. In particular, the adopted six (nine) model parameters are listed in Table 8 (9).

Looking at Tables 8 and 9, we can observe that the proposed model needs a smaller number of parameters than the Modified Bouc-Wen Model. In addition, since such parameters have a clear graphical meaning, as shown in 4.2.5, we may point out that the proposed model requires a simplified parameters identification procedure.

5.6. Results of the nonlinear time history analyses

We now present the numerical results of the nonlinear time history analyses to demonstrate the numerical accuracy and the computational efficiency of the Asymmetric Exponential Model.

To perform such analyses, we have numerically solved Eq. (85) by employing an explicit structure-dependent time integration method [15,35] and adopting a time step of 0.001 s. Furthermore, we have numerically solved Eq. (87), that characterizes the Modified Bouc-Wen Model, by means of the unconditionally stable semi-implicit Runge–Kutta method [27] and using 50 steps. The solution algorithms have been implemented in the computer program MATLAB and run on a computer having an Intel® Core™ i7-4700MQ processor and a CPU at 2.40 GHz with 16 GB of RAM.

Table 10 (11) presents the Nonlinear Time History Analyses (NLTHAs) results obtained by applying the harmonic force (random force). We can observe that the accuracy of the Asymmetric Exponential Model is very satisfactory; indeed, such a model gives maximum and minimum values of the generalized displacements, velocities, and accelerations that are quite close to those evaluated by employing the Modified Bouc-Wen Model. In addition, the accuracy of the proposed model is also confirmed by Figs. 17–19 that illustrate, respectively, the time histories of the generalized displacement, velocity, and acceleration, as well as the generalized force-displacement hysteresis loops, simulated by both the asymmetric models. (see Fig. 20).

Finally, as far as the computational efficiency is concerned, Tables 10 and 11 provide the total computational time *tct* and the total computational time percentage *tctp* of the proposed model, evaluated as:

$$\text{AEM } tctp\ [\%] = \frac{\text{AEM } tct}{\text{MBWM } tct} \cdot 100. \tag{88}$$

These values confirm the computational efficiency of the Asymmetric Exponential Model that clearly allows us to drastically reduce the computational burden of the nonlinear time history analyses.

6. Conclusions

We have reformulated a class of uniaxial rate-independent hysteretic models, originally developed by Vaiana et al. [33], to reproduce generalized force–displacement hysteresis loops characterized by asymmetric shapes. Subsequently, we have developed two instances of such a class, denominated Asymmetric Bilinear Model and Asymmetric Exponential Model, in order to better illustrate the meaning of the quantities employed in the reformulation and to show its properties in terms of accuracy and computational efficiency.

The Asymmetric Exponential Model, capable of simulating six different types of generalized force-displacement hysteresis loop shape, namely two symmetric and four asymmetric shape types, has been experimentally and numerically verified.

The experimental verification reveals that the proposed model is able to accurately reproduce the highly asymmetric experimental hysteresis loops displayed by some spring connectors tested by Filiatrault and Kremmidas [13]. Furthermore, compared to the Generalized Bouc-Wen Model, specifically developed by Song and Der Kiureghian [31] to simulate the complex experimental behavior of such devices, the proposed model turns out to be more accurate by using a smaller set of parameters. Actually, the Asymmetric Exponential Model is able to well simulate the increase of the transverse tangent stiffness observed for increasing positive values of the transverse displacement by using six, rather than ten, parameters. Furthermore, the adopted six parameters have a specific graphical meaning, as shown in 4.2.5.

The numerical verification, performed by carrying out some nonlinear time history analyses on a rate-independent mechanical system having asymmetric hysteretic behavior, reveals that the Asymmetric Exponential Model not only provides results that are very close to those predicted by using the Modified Bouc-Wen Model formulated by Ref. [23], but it also allows for the reduction of the computational times. Indeed, it requires only the 0.66% (0.69%) of the time required

Please cite this article as: N. Vaiana, S. Sessa and L. Rosati, A generalized class of uniaxial rate-independent models for simulating asymmetric mechanical hysteresis phenomena, Mechanical Systems and Signal Processing, https://doi.org/10.1016/j.ymssp.2020.106984

by the Modified Bouc-Wen Model when the analyses are performed by applying the generalized external harmonic (random) force.

Current research is focusing on the extension of the proposed general formulation to the case of cyclic hardening and softening, by assuming the adopted parameters as functions of other quantities, such as the hysteresis loop area or the number of cycles, and to the case of pinching phenomena, by conveniently modifying the general expression of the generalized tangent stiffness function.

Declaration of Competing Interest

The authors declare that they have no known competing financial interests or personal relationships that could have appeared to influence the work reported in this paper.

CRediT authorship contribution statement

Nicolò Vaiana: Conceptualization, Methodology, Software, Validation, Writing - original draft, Writing - review & editing. **Salvatore Sessa:** Supervision. **Luciano Rosati:** Writing - review & editing, Supervision, Project administration, Funding acquisition.

Acknowledgments

The authors acknowledge the Italian Government (ReLUIS 2017 project [AQ DPC/ReLUIS 2014–2018, PR2, Task 2.3] and PRIN 2015 grants [2015JW9NJT-PE8, WP2, Task 2.1]) for supporting the present research.

References

[1] G. Aguirre, T. Janssens, H. Van Brussel, F. Al-Bender, Asymmetric-hysteresis compensation in piezoelectric actuators, Mechanical Systems and Signal Processing 30 (2012) 218–231.
[2] M. Alam, M. Youssef, M. Nehdi, Utilizing shape memory alloys to enhance the performance and safety of civil infrastructure: a review, Canadian Journal of Civil Engineering 34 (2007) 1075–1086.
[3] S. Alessandri, R. Giannini, F. Paolacci, M. Amoretti, A. Freddo, Seismic retrofitting of an HV circuit breaker using base isolation with wire ropes. Part 2: Shaking-table test validation, Engineering Structures 98 (2015) 263–274.
[4] S. Alessandri, R. Giannini, F. Paolacci, M. Malena, Seismic retrofitting of an HV circuit breaker using base isolation with wire ropes. Part 1: Preliminary tests and analyses, Engineering Structures 98 (2015) 251–262.
[5] V. Anes, Y. Lage, M. Vieira, N. Maia, M. Freitas, L. Reis, Torsional and axial damping properties of the AZ31B-F magnesium alloy, Mechanical Systems and Signal Processing 79 (2016) 112–122.
[6] G. Bertotti, I. Mayergoyz, The Science of Hysteresis, Academic Press, 2005.
[7] R. Bouc, Modèle mathématique d'hystérésis, Acustica 24 (1971) 16–25.
[8] G. Demetriades, M. Constantinou, A. Reinhorn, Study of wire rope systems for seismic protection of equipment in buildings, Engineering Structures 15 (1993) 321–334.
[9] M. Dimian, P. Andrei, Noise-Driven Phenomena in Hysteretic Systems, Springer, New York, NY, USA, 2014.
[10] S. Dobson, M. Noori, Z. Hou, M. Dimentberg, T. Baber, Modeling and random vibration analysis of SDOF systems with asymmetric hysteresis, International Journal of Non-Linear Mechanics 32 (1997) 669–680.
[11] M. Dolce, D. Cardone, R. Marnetto, Implementation and testing of passive control devices based on shape memory alloys, Earthquake Engineering and Structural Dynamics 29 (2000) 945–968.
[12] P. Duhem, Die dauernden aenderungen und die thermodynamik, I. Zeitschrift für Physikalische Chemie 22 (1897) 545–589.
[13] A. Filiatrault, S. Kremmidas, Seismic interaction of interconnected electrical substation equipment, Journal of Structural Engineering, ASCE 126 (2000) 1140–1149.
[14] R. Gerges, Model for the force-displacement relationship of wire rope springs, Journal of Aerospace Engineering, ASCE 21 (2008) 1–9.
[15] F. Greco, R. Luciano, G. Serino, N. Vaiana, A mixed explicit-implicit time integration approach for nonlinear analysis of base-isolated structures, Annals of Solid and Structural Mechanics 10 (2018) 17–29.
[16] Q. Han, M. Hu, K. Xu, X. Du, Hysteretic behavior and modelling of ultra-high-strength steel bar including buckling, Bulletin of Earthquake Engineering 17 (2019) 5265–5289.
[17] S.Y. Kim, C.H. Lee, Description of asymmetric hysteretic behavior based on the Bouc-Wen model and piecewise linear strength-degradation functions, Engineering Structures 181 (2019) 181–191.
[18] Y. Liu, Z. Xie, J. Van Humbeeck, Cyclic deformation of NiTi shape memory alloys, Materials Science and Engineering: A 273–275 (1999) 673–678.
[19] D. Losanno, I. Madera Sierra, M. Spizzuoco, J. Marulanda, P. Thomson, Experimental assessment and analytical modeling of novel fiber-reinforced isolators in unbounded configuration, Composite Structures 212 (2019) 66–82.
[20] I. Madera Sierra, D. Losanno, S. Strano, J. Marulanda, P. Thomson, Development and experimental behavior of HDR seismic isolators for low-rise residential buildings, Engineering Structures 183 (2019) 894–906.
[21] A. Malher, O. Doaré, C. Touzé, Influence of a hysteretic damper on the flutter instability, Journal of Fluids and Structures 68 (2017) 356–369.
[22] G. Monti, C. Nuti, Nonlinear cyclic behavior of reinforcing bars including buckling, Journal of Structural Engineering, ASCE 118 (1992) 3268–3284.
[23] Y. Ni, J. Ko, C. Wong, S. Zhan, Modelling and identification of a wire-cable vibration isolator via a cyclic loading test. Part 1: Experiments and model development, Journal of Systems and Control Engineering 213 (1999) 163–171.
[24] A. Piersol, T. Paez, Harris' Shock and Vibration Handbook, sixth ed., McGraw-Hill, New York, NY, USA, 2010.
[25] A. Quarteroni, R. Sacco, F. Saleri, Numerical Mathematics, Springer-Verlag, New York, NY, USA, 2000.
[26] J. Rodgers, S. Mahin, Effects of connection deformation softening on behavior of steel moment frames subjected to earthquakes, International Journal of Steel Structures 11 (2011) 29–37.
[27] H. Rosenbrock, Some general implicit processes for the numerical solution of differential equations, The Computer Journal 4 (1963) 329–330.
[28] S. Sessa, F. Marmo, N. Vaiana, L. Rosati, A computational strategy for Eurocode 8 - compliant analyses of reinforced concrete structures by seismic envelopes, Journal of Earthquake Engineering (2018), https://doi.org/10.1080/13632469.2018.1551161.

Please cite this article as: N. Vaiana, S. Sessa and L. Rosati, A generalized class of uniaxial rate-independent models for simulating asymmetric mechanical hysteresis phenomena, Mechanical Systems and Signal Processing, https://doi.org/10.1016/j.ymssp.2020.106984

[29] S. Sessa, N. Vaiana, M. Paradiso, L. Rosati, An inverse identification strategy for the mechanical parameters of a phenomenological hysteretic constitutive model, Mechanical Systems and Signal Processing 139 (2020), 106622.
[30] M. Sivaselvan, A. Reinhorn, Hysteretic models for deteriorating inelastic structures, Journal of Engineering Mechanics, ASCE 126 (2000) 633–640.
[31] J. Song, A. Der Kiureghian, Generalized Bouc-Wen model for highly asymmetric hysteresis, Journal of Engineering Mechanics, ASCE 132 (2006) 610–618.
[32] M. Tinker, M. Cutchins, Damping phenomena in a wire rope vibration isolation system, Journal of Sound and Vibration 157 (1992) 7–18.
[33] N. Vaiana, S. Sessa, F. Marmo, L. Rosati, A class of uniaxial phenomenological models for simulating hysteretic phenomena in rate-independent mechanical systems and materials, Nonlinear Dynamics 93 (2018) 1647–1669.
[34] N. Vaiana, S. Sessa, F. Marmo, L. Rosati, An accurate and computationally efficient uniaxial phenomenological model for steel and fiber reinforced elastomeric bearings, Composite Structures 211 (2019) 196–212.
[35] N. Vaiana, S. Sessa, F. Marmo, L. Rosati, Nonlinear dynamic analysis of hysteretic mechanical systems by combining a novel rate-independent model and an explicit time integration method, Nonlinear Dynamics 98 (2019) 2879–2901.
[36] N. Vaiana, M. Spizzuoco, G. Serino, Wire rope isolators for seismically base-isolated lightweight structures: experimental characterization and mathematical modeling, Engineering Structures 140 (2017) 498–514.
[37] A. Visintin, On hysteresis in elasto-plasticity and in ferromagnetism, International Journal of Non-Linear Mechanics 37 (2002) 1283–1298.
[38] C.H. Wang, Y.K. Wen, Reliability and redundancy of pre-Northridge low-rise steel buildings under seismic excitation. UILU-ENG-99-2002, SRS No. 624, University of Illinois, Urbana, IL, USA, 1998. .
[39] Y.K. Wen, Method for random vibration of hysteretic systems, Journal of the Engineering Mechanics Division, ASCE 102 (1976) 249–263.
[40] Y.K. Wen, Equivalent linearization for hysteretic systems under random excitation, Journal of Applied Mechanics, ASME 47 (1980) 150–154.
[41] S. Yi, B. Yang, G. Meng, Microvibration isolation by adaptive feedforward control with asymmetric hysteresis compensation, Mechanical Systems and Signal Processing 114 (2019) 644–657.
[42] B. Zhang, Z. Lang, S. Billings, G. Tomlinson, J. Rongong, System identification methods for metal rubber devices, Mechanical Systems and Signal Processing 39 (2013) 207–226.
[43] Z. Zhou, Y. Tan, X. Liu, State estimation of dynamic systems with sandwich structure and hysteresis, Mechanical Systems and Signal Processing 126 (2019) 82–97.

Please cite this article as: N. Vaiana, S. Sessa and L. Rosati, A generalized class of uniaxial rate-independent models for simulating asymmetric mechanical hysteresis phenomena, Mechanical Systems and Signal Processing, https://doi.org/10.1016/j.ymssp.2020.106984